NTNU

Norwegian University of
Science and Technology

Measurements of Optical Penetration Depth in Smoked Salmon

Remi Andre Ursin Johansen

Master of Science in Electronics
Submission date: June 2008
Supervisor: Astrid Aksnes, IET
Co-supervisor: Lise Lyngsnes Randeberg, IET
Eivind La Puebla Larsen, IET

Norwegian University of Science and Technology
Department of Electronics and Telecommunications

Problem Description

The thesis includes measurements of optical properties in smoked Atlantic salmon, and should contain the following parts:

1.Rebuilding and stability testing of an existing equipment for fluence rate measurements. Use of the setup to find the optical penetration depth of smoked salmon at 632nm. Modification of the system to include measurements at 532nm.
2.Construction of a setup to measure fluence rate using a white light source and a fiber optic spectrometer. Use of this equipment to measure the penetration depth of smoked salmon in the wavelength region 400-800nm.
3.Calibration of the measurements using Intralipid and ink, and calculation of the absorption- and scattering coefficients of the fish.

Assignment given: 28. January 2008
Supervisor: Astrid Aksnes, IET

Preface

This master's thesis has been written as a part of the graduate course, TFE4920 Master's thesis, at the Norwegian University of Science and Technology (NTNU), Department of Electronics and Telecommunications, during the spring of 2008.

This has been my most demanding, but also my most informative semester. I have experienced the world of research, which has been both frustrating and interesting. I would like to thank my supervisors Astrid Aksnes, Lise Lyngsnes Randeberg and Eivind La Puebla Larsen for giving me the opportunity to work with this thesis. They have supported me and contributed with their expert knowledge. Their feedback has motivated me and made me work harder. Without them this thesis could not have been written. I would also like to thank Torbjørn Andersen Ve for inspiring and helpful discussions. His critical reading has contributed to making this thesis better.

Abstract

Optical spectroscopy is a common method used in the determination of quality parameters in groceries. An optical characterization of smoked Atlantic salmon was carried out in this thesis. The optical penetration depth in salmon was found at 531 nm and 632 nm from measurements with lasers as light sources, and from 550 nm to 880 nm with a tungsten halogen lamp as light source. The spectrum of the halogen lamp combined with the absorption spectrum of the salmon made it difficult to obtain results for wavelengths below 550 nm with the halogen lamp. Two variations in the measurements on smoked salmon were performed; measuring on needle insertion versus needle extraction and measuring across several layers of muscle tissue versus measuring along one layer of muscle tissue in salmon. The absorption coefficient and the reduced scattering coefficient of smoked Atlantic salmon was calculated. Significant differences were found dependent on needle insertion or needle extraction, and whether the measurements were made along one layer or across several layers. The penetration depths were found to be 6.79 ± 0.33 mm across several layers and 10.76 ± 1.03 mm along one layer in the measurements with the He-Ne laser. The diffusion approximation was found to be a good approximation for wavelengths from 600 nm to 700 nm. With further development, it may be possible to determine the astaxanthin content of salmon with the method used in this thesis.

Contents

1 Introduction

Optical spectroscopy is a common method used in the determination of quality parameters in groceries. Beef is of current interest, and attempts to determine the tenderness have been performed [1]. Fat and protein contents of cheese have also been investigated [2] [3]. Fish, chicken and dairy products are other relevant groceries to investigate by the use of spectroscopy.

In 2006, the seafood industry was responsible for 5 per cent of Norway's total export revenues. Seafood is thus one of Norway's most important export industries. Salmon and trout accounted for 52 per cent of the export of seafood in 2006[4]. The development of objective methods to determine quality parameters in salmon is therefore important. The authors personal interest in salmon also contributed to the choice of salmon.

The color and the fat content are two important quality parameters in salmon[5]. Methods for rapid determination of these parameters is desirable, and spectroscopy is a viable alternative. The fat content have been found by the use of near infra-red spectroscopy[6][7]. Diffuse reflection spectroscopy in the short wave near infra-red part of the spectrum has been used to determine the salt and moisture content[8][9]. Color analysis have been made to determine the astaxanthin content which gives the red color to the salmon. The analysis consisted of using a colorimeter and color cards, and the results were compared with astaxanthin content found from chemical analysis[10]. It was concluded that the use of a colorimeter and color cards were less useful in measuring the concentration of astaxanthin in individual fillets. To the authors knowledge, few attempts have been made to determine the astaxanthin content in salmon by spectroscopy. Raman spectroscopy is one of the attempts to determine the astaxanthin content by the use of spectroscopy[11].

In this thesis transmission spectroscopy is used to determine the optical properties of smoked salmon. The diffusion approximation in radiative transfer theory has been used in calculating μ_a and μ_s' in the visible spectrum. The calculations are based on the penetration depths obtained from non-destructive measurements, and calibration from measurements on intralipid and ink. This thesis also compares variations in how the measurements on salmon are performed. Hopefully the results will contribute to the development of a method to utilize the visible spectrum to determine some of the quality parameters of salmon.

Relevant theory is presented in section 2. The description of the setup and measurement procedures, and the explanation of the data analysis is presented in section 3. The results are presented in section 4, and disussed in section 5.

2 Theory

The behaviour of light is described by Maxwell's equations. If the system analyzed is simple, Maxwell's equations are the best alternative because the properties of light are preserved during the calculations. In this thesis salmon is studied. A salmon represents a complex system which is not possible to analyze using Maxwell's equations. Different approximation methods have been developed in the place of Maxwell's equations. These methods include for instance the Kubelka-Munk model and the diffusion approximation in radiative transport theory [12]. The analysis done in this thesis is based on the diffusion approximation.

2.1 Absorption and scattering of light

Consider a collimated photon beam through a slab of material with infinitesimal thickness $\mathrm{d}x$. The attenuation may be described as[13]

$$\mathrm{d}I = -N\sigma I \mathrm{d}x, \tag{1}$$

where I is the number of photons per second, N is the number density of the interacting molecules in the material and σ is the interaction cross section. Suppose a non-scattering material, where $\sigma = \sigma_a$ is the absorption cross section. Solving eq. (1) yields

$$I(x) = I_0 e^{-\mu_a x}, \tag{2}$$

where I_0 is the number of photons incident on the material at $x = 0$ and $\mu_a = N\sigma_a$ is the absorption coefficient. This equation is referred to as Beer's law[14][15]. Supposing the material is scattering and non-absorbing, a corresponding deduction may be carried out, and the scattering coefficient is defined as $\mu_s = N\sigma_s$. When both absorption and scattering are present, Beer's law takes the form

$$I(x) = I_0 e^{-\mu_t x}, \tag{3}$$

where $\mu_t = \mu_a + \mu_s$ is the total attenuation coefficient. The validity of Beer's law is limited to small scattering contributions and low concentrations of absorbing particles [16] [17]. Thus, Beer's law is not a suitable description of light distribution in turbid media. In the description of a scattering incidence, the scattering angle is of importance when describing the light distribution. The scattering anisotropy g is defined as the average of the cosine to the scattering angle, $g = \overline{\cos\theta}$, where θ is the scattering angle. $\mu_s' = \mu_s(1-g)$ is the reduced scattering coefficient. The transport mean free path, l_{tr}, is the distance over which the photons loses its initial direction[18][19]:

$$l_{tr} = \frac{1}{\mu_a + \mu_s'}. \tag{4}$$

2.2 Radiometric quantities

Radiative transport theory describes the transfer of energy in turbid media, e.g. biological material. When describing the transfer of energy the most important quatities are; radiant power, radiant intensity, radiance and fluence rate. These quantities have standard definitions, and are given below[20]

Radiant power P

Definition: The power emitted, transferred or received as radiation.

Unit: $[P]$=W

Radiant intensity I

Definition: In a given direction from a source, the radiant intensity is defined by the radiant power $\mathrm{d}P$ leaving the source in an element of solid angle $\mathrm{d}\Omega$ containing this direction, divided by that element of solid angle:

$$I = \frac{\mathrm{d}P}{\mathrm{d}\Omega} \tag{5}$$

Unit: $[I]$= $\frac{\mathrm{W}}{\mathrm{sr}}$

Radiance L

Definition: At a point on a surface and in a given direction, the radiance L is given by the radiant intensity $\mathrm{d}I$ of an element $\mathrm{d}A$ of the surface, divided by the area of the orthogonal projection of this element on a plane perpendicular to the given direction:

$$L = \frac{\mathrm{d}I}{\mathrm{d}A\cos\theta} \tag{6}$$

Unit: $[L]$= $\frac{\mathrm{W}}{\mathrm{sr}\cdot\mathrm{m}^2}$

Fluence rate ϕ

Definition: At a given point in space, the fluence rate ϕ is the radiant intensity incident on a small sphere divided by the cross-sectional area of the sphere. It is given by the integral over the radiance at that point, taken over 4π solid angle:

$$\phi(\mathbf{r}) = \int_{4\pi} L(\Omega, \mathbf{r}) d\Omega \tag{7}$$

Unit: $[\phi]= \frac{\mathrm{W}}{\mathrm{m}^2}$

2.3 Diffusion approximation

Beer's law is useful in describing the light transport, but it is limited to low scattering which is not the case with turbid media. Boltzmann's transport equation may be used to describe the behaviour of the light in cases of dominant scattering. Even though Boltzmann's transport equation is possible to solve analytically for a few cases[21], approximations are often needed to obtain a new set of feasible equations. For a low frequency signal it is sufficient to treat the light transport as a stationary case[22]. The stationary Boltzmann's transport equation is given by[21]

$$\nabla \cdot [\mathbf{s}L(\mathbf{r},\mathbf{s})] = -\mu_t L(\mathbf{r},\mathbf{s}) + \mu_s \int_{4\pi} L(\mathbf{r},\mathbf{s})p(\mathbf{s},\mathbf{s'})\mathrm{d}\Omega' + Q(\mathbf{r},\mathbf{s}), \tag{8}$$

where $L(\mathbf{r},\mathbf{s})$ is the radiant intensity at point $\mathbf{r}$ in direction $\mathbf{s}$, $Q(\mathbf{r},\mathbf{s})$ is the source intensity, $p(\mathbf{s},\mathbf{s'})$ is the phase function and $\mathbf{s'}$ is the direction of the incident photons. The transport equation describes the conservation of energy within a defined volume element at $\mathbf{r}$. $\nabla \cdot [\mathbf{s}L(\mathbf{r},\mathbf{s})]$ represents the power in direction $\mathbf{s}$ in a volume at $\mathbf{r}$. $\mu_t L(\mathbf{r},\mathbf{s})$ represents the loss of power due to absorption, and due to scattering out of direction $\mathbf{s}$. $\mu_s \int_{4\pi} L(\mathbf{r},\mathbf{s})p(\mathbf{s},\mathbf{s'})d\Omega'$ respresents the power deflected from direction $\mathbf{s'}$ into direction $\mathbf{s}$. $Q(\mathbf{r},\mathbf{s})$ represents power injected in the direction $\mathbf{s}$ at the volume element at $\mathbf{r}$. If scattering is dominant over absorption, the radiance may be expressed using spherical harmonics [23]. Only including the two first terms in the spherical harmonics yields

$$L = \frac{1}{4\pi}\phi + \frac{3}{4\pi}\mathbf{j} \cdot \mathbf{s}, \tag{9}$$

where the fluence rate , ϕ, is the isotropic term, and the flux , $\mathbf{j}$, is the directional perturbation term. By substituting eq. (9) into eq. (8) integrating over all solid angles using,

- $\int_{4\pi} \mathbf{s}L(\mathbf{r},\mathbf{s})\mathrm{d}\Omega = \mathbf{j}$,
- $\int_{4\pi} p(\mathbf{s},\mathbf{s'})\mathrm{d}\Omega = 1$,
- $\int_{4\pi} Q(\mathbf{r},\mathbf{s})\mathrm{d}\Omega = q$,

and the definition of ϕ, eq. (7), a continuity equation is obtained[14][24]:

$$\nabla \mathbf{j} = q - \mu_a \phi. \tag{10}$$

The leakage rate out of the volume, $\nabla \cdot \mathbf{j}$, equals the production rate, q, minus the absorption rate within the volume, $\mu_a\phi$. Substituting eq. (9) into eq. (8), multiplying with $\mathbf{s}$ and integrating over all solid angles yields Fick's law for photons[24]

$$\mathbf{j} = -\xi \nabla \phi, \tag{11}$$

$\xi = l_{tr}/3$ is the diffusion coefficient. Q is assumed to be isotropic. By taking the divergence of eq. (11) and substituting into eq. (10), a differential equation for the fluence rate is obtained[14]

$$\nabla^2\phi - \frac{\phi}{\delta^2} = -\frac{q}{\xi}, \tag{12}$$

where δ is the penetration depth given as[14]

$$\delta = \left(\frac{1}{3\mu_a(\mu_a + \mu_s')}\right)^{1/2}. \tag{13}$$

Assuming $q \approx 0$[25] and using spherical coordinates, the solution to eq. (12) is[13]

$$\phi(r) = B\frac{e^{-\delta^{-1}r}}{r} + C\frac{e^{\delta^{-1}r}}{r}, \tag{14}$$

where r is the distance from the imagined point source, see figure 1. B and C are constants, and as r approaches infinity the fluence rate approaches zero, implying $C = 0$. Setting $C = 0$ leaves

$$\phi(r) = B\frac{e^{-\delta^{-1}r}}{r}, \tag{15}$$

The approximations in this thesis assumes an infite turbid medium (i.e. no boundaries

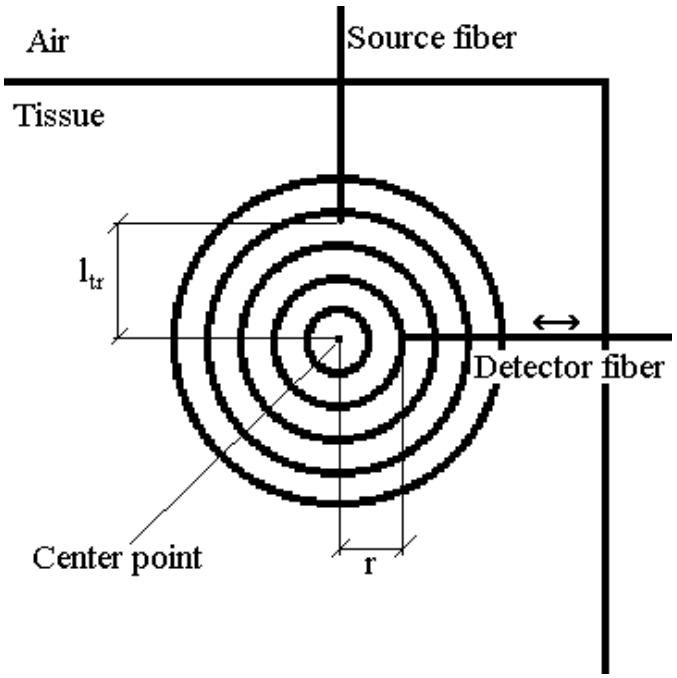

Figure 1: Illustration of the imagined source

are accounted for). $\mu_a << \mu_s'$ is stated as a criterion for the validity of the diffusion

approximation[26]. In the requirement of an isotropic source, it is assumed that the imagined point source forms a certain distance, l_{tr}, in front of the source fiber[24]. This is illustrated in figure 1. The signal detected is assumed to be proportional to the fluence rate. Assuming no source terms in eq. (12) simplifies the calculations, but limits the validity of the approximations where the distance from the source is small compared to the penetration depth[25]. Neglecting the source term also assumes that no inelastic scattering is taking place.

Multiplying eq. (15) by r, and taking the natural logarithm leaves

$$\ln(r\phi) = -\delta^{-1}r + \ln(B). \tag{16}$$

If $\ln(r\phi)$ is plotted as a function of distance, r, δ can be found by a linear fit.

2.4 Salmon

The tissue in salmon is not homogenous. On the microscopic scale it consists of muscle fibers and fat among others. These elements have different refractive indicies leading to scattering of the light. On the macroscopic scale the salmon tissue is clearly divided in layers, see figure 2. This may affect the optical properties of salmon. Astaxanthin is responsible for the red coloration of the flesh. The salmon is not able to produce ataxanthin itself. It is included in the fodder for the farmed salmon, whilst wild salmon receives it through the diet[27]. Astaxanthin limits the validity of the diffusion approximation in the shorter wavelengths, as the absorption is significant. The spectrum for astaxanthin is shown in figure 3.

Figure 2: Photograph of a salmon indicating the divison in several layers

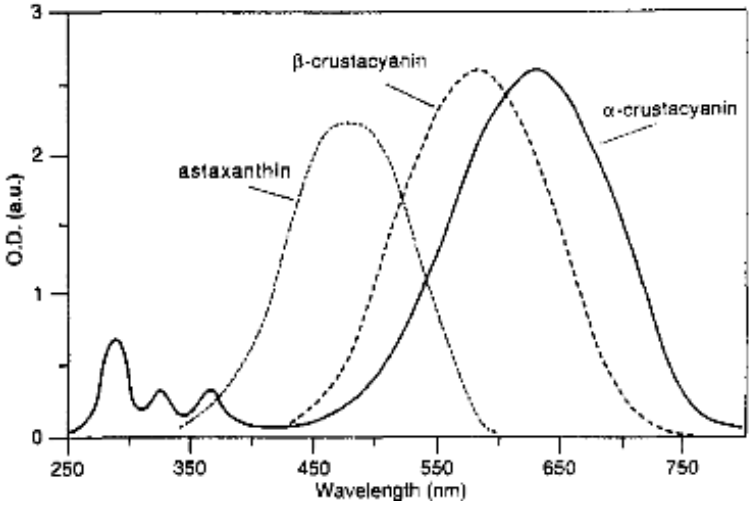

Figure 3: UV/Visible spectra of astaxanthin (in dimethylformamide) and of α-crustacyanin and β-crustacyanin (in $0.05M$ sodium phosphate pH 7.0)[28].

3 Method

In the measurements with the lasers, a lock-in amplifier was used to suppress noise, a technique which has been used before[29][30]. In the process of finding μ_s' and μ_a for intralipid, the added absorber technique was used[31]. The added absorber was china ink. A similar approach was used when finding μ_s' and μ_a for the salmon. Mashed salmon was mixed with intralipid. $\mu'_{s,intralipid}$ was known and $\mu_{a,intralipid} << \mu_{a,salmon}$ was assumed. Combined with the measurement on salmon it was possible to calculate $\mu_{a,salmon}$ and $\mu'_{s,salmon}$. Measurements were done in intervals of 1 mm in the distance between the source fiber and the detector fiber. The distances ranged from 3 mm to 25 mm for the lasers and 5 mm to 20 mm for the halogen lamp.

3.1 Setup for the lasers

The setup is shown in figure 4. The voltage applied to the Photon Multiplier Tube (PMT) was 800 V. The pre-amplifier had a power supply from two 9 V batteries. The amplification was set to 10^5 V/A in the first experiments. It was later changed to 10^4 V/A. The frequency of the chopper was set to 1000 Hz, but fluctuated between 975 Hz and 1010 Hz. The integration time on the lock-in amplifier was set to 0.3 seconds. The sensitivity was changed during the experiments, and a lower sensitivity was used for shorter distances between the detector fiber and the source fiber. The oscilloscope was used to monitor the reference signal and the measuring signal. The measurements were read directly from the lock-in amplifier. The spectrum and the stability of the lasers were measured, and the results are given in the appendix. Table 1 shows information about the lasers used. Table 2 shows the movability of the sample holder, the source fiber and the detector fiber. The fibers used in the experiments are shown in table 3

Table 1: Lasers used in the experiments

Type of laser	Effect at peak wavelength (mW)	Peak wavelength (nm)	FWHM (nm)	Minimum warm up time used (minutes)
Helium-Neon	6	631.79	5.68	15
YAG	18	531.24	7.46	60

3.2 Setup for the halogen lamp

A casing of black paperboard was built around the sample holder to minimize the stray light. Only the lower part of this case is shown in the photograph of the setup, figure 5. A lens integrated in the casing for the halogen lamp focused the light into the source fiber. The source fiber and the detector fiber were connected by a connector to the lamp and the spectrometer, respectively. The spectrometer was connected to a computer, and adjustments were done through the pertaining software. Correction for the electric dark

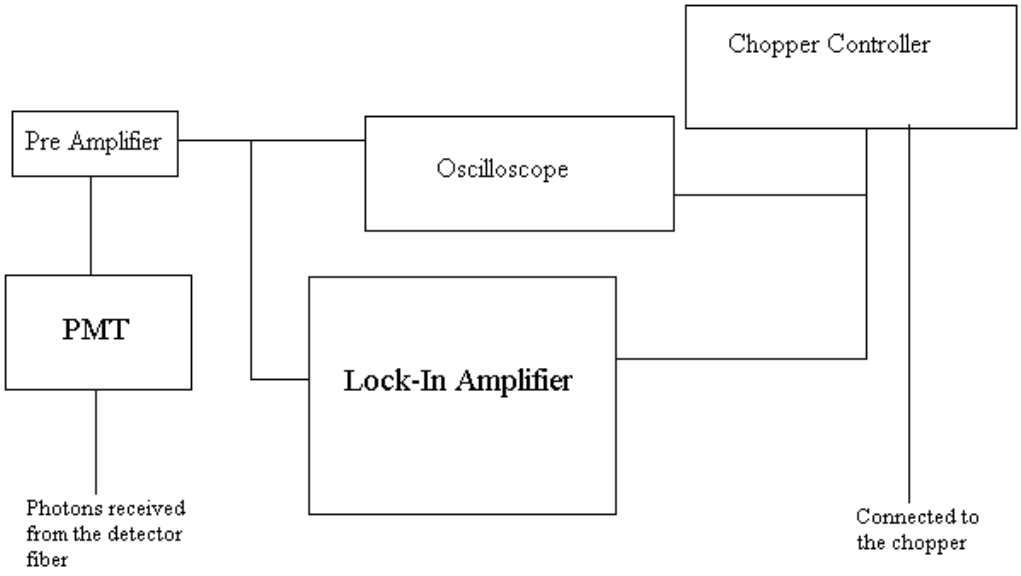

(a) Instruments.

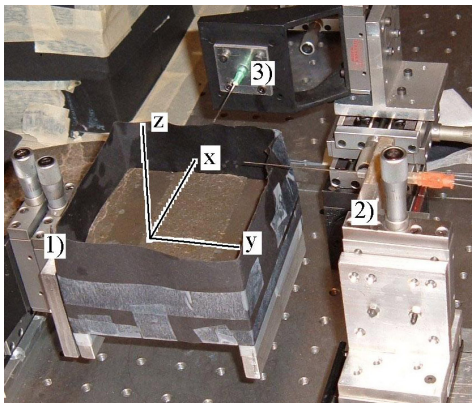

(b) 1) Sample holder, 2) Detector fiber, 3) Source fiber. Table 2 shows the movability of these components.

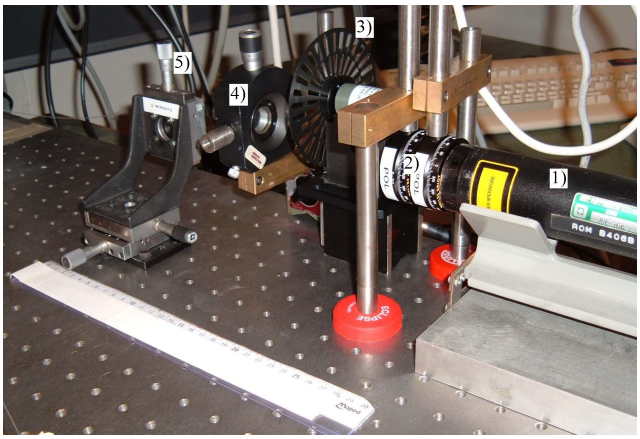

(c) 1) Laser (He-Ne in this photograph), 2) Polarizers, 3) Chopper, 4) Focusing lens (NA=0.25), 5) Source fiber end where the light is coupled in. The length of the ruler on the photograph was 300 mm.

Figure 4: Setup used in the measurements with the lasers

Table 2: Movability of the sample holder, source fiber and detector fiber using the defined directions in figure 4(b)

Component	x-direction (mm)	y-direction (mm)	z-direction (mm)
Sample holder	0	15	30
Detector fiber	15	25	15
Source fiber	30	15	15

Table 3: Fibers used in the experiments with the lasers.

Fiber	Core diameter (μm)	Length (m)	Producer	NA	Model
Detector fiber	200	0.5-1	Thorlabs	0.22	FG-200-LCR
Source fiber	400	0.5-1	Thorlabs	0.16	FG-400-UAT

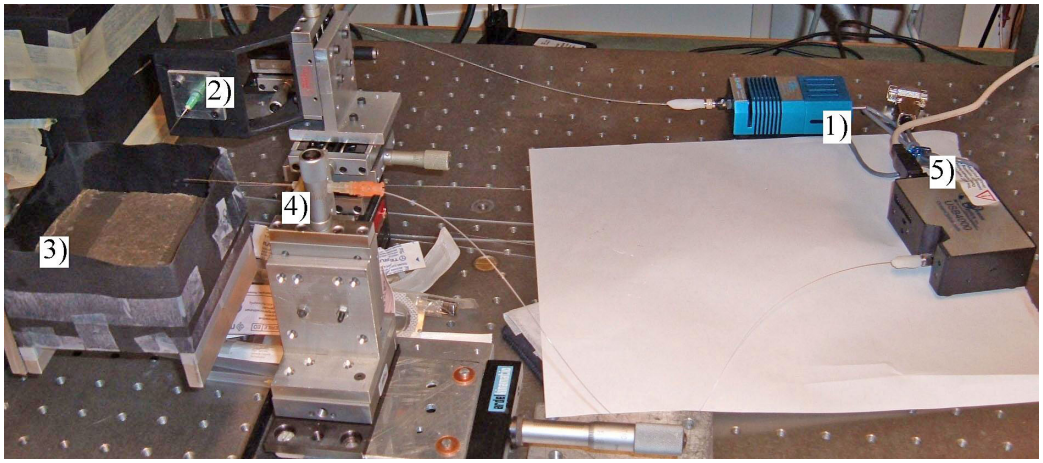

Figure 5: Photograph of the setup used in measurements with the halogen lamp. 1) Halogen lamp, 2) source fiber, 3) sample holder, 4) detector fiber, 5) spectrometer.

current was done using the software. The integration time was set to 5 seconds, and the average of three measurements were used. Boxcar width in the software was set to 3. A dark reference spectrum was registered, and subtracted from all the measurements. All measurements were stored as ASCII-files on the computer. The spectrum of the halogen lamp is shown in figure 6. The fibers used in the experiments are shown in table 4. An overview of the instruments used in the setup for both the lasers and the halogen lamp are shown in table 5, and technical specifications for most of the instruments are found in the appendix.

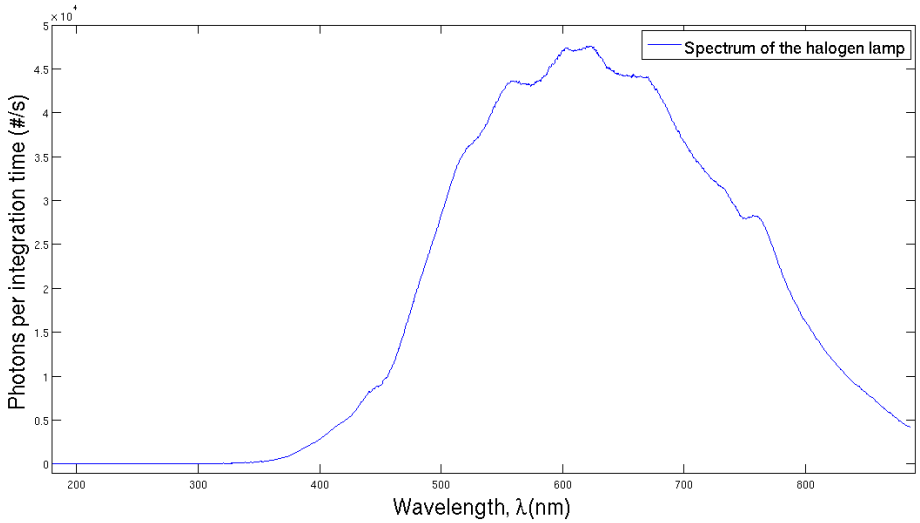

Figure 6: Spectrum of the halogen lamp

Table 4: Fibers used in the experiments with the halogen lamp.

Fiber	Core diameter (μm)	Length (m)	Producer	NA	Model
Detector fiber	200	0.5-1	Thorlabs	0.37	BFH37-200
Source fiber	400	0.5-1	Thorlabs	0.48	BFH48-400

3.3 Measurement procedures

The detector and source fibers were glued to the needle. The fiber ends were about 0.5 mm outside the tip of their respective needles. In the measurements with the halogen lamp the fibers were changed. This may have changed the length of the fiber outside the needles. The detector fiber was contained in two needles to increase the stiffness. A photograph of the detector needle is shown in figure 7. Information about the needles used in the setup are shown in table 6.

Table 5: The instruments used in the experiments.

Instrument	Producer	Model
PMT	Oriel	7070
Pre Amplifier	Made at NTNU	-
Oscilloscope	Tektronix	2445
Chopper Controller	Stanford Research Systems	SR540
Lock-In Amplifier	Stanford Research Systems	SR830 DSP
He-Ne laser	Research Electro Optics	30990
YAG laser	Shanghai Dream Laser Technology	SDL-532-010-SLM
Tungsten Halogen Lamp	Ocean Optics	LS-1
Fiber Optic Spectrometer	Ocean Optics	USB4000
Spectrasuite (software)	Ocean Optics	v 5.1, Windows XP

Table 6: Needles used in the experiments

Item	Size	Length (mm)	Producer
Inner detector needle	25 G	90	Yale
Outer detector needle	19 G	31	Terumo
Source needle	21 G	40	Terumo
Needle in the beaker	19 G	19	Terumo

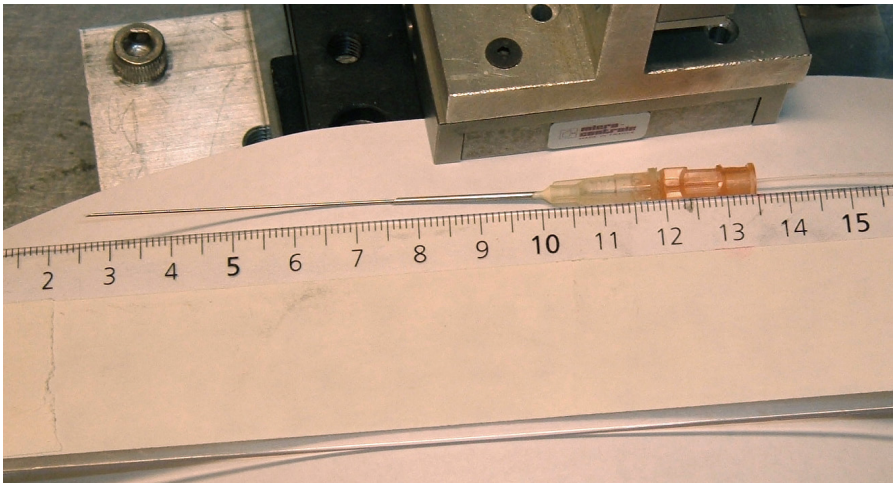

Figure 7: The detector needles.

3.3.1 Fluids

Measurements were done on four solutions. The concentration of intralipid were 250mg per 100mL (0.25%) in all solutions, and three of the solutions also contained other elements, see table 7. Solution number 4 was mixed by a handblender (Braun, Multiquick MR430). In the measurements, the fluids were kept in a beaker with two holes drilled in it. The holes were sealed by five alternating layers of sports tape and aluminium tape. Another needle (denoted "Needle in the beaker" in table 6) was inserted into one of the holes. In the measurements the detector needle was inserted and extracted through this needle. This was done to minimize the friction for the detector needle. A photograph of the beaker in the sample holder with the detector needle inserted through the needle in the beaker is shown in figure 8(b). Two photgraphs of the beaker are shown in figure 8.

Table 7: Fluids used in the measurements.

Solution nr	China Ink (μL)	Mashed Salmon (g)	Total volume (mL)
1	0	0	240
2	15	0	240
3	30	0	240
4	0	20.6	259

3.3.2 Salmon

Smoked salmon was chosen over unprocessed salmon due to better keeping quality. The producer of the salmon was Godehag, Norway. The measurements on the salmon were done in four separate parts; when inserting needle across several layers, when extracting

(a) Beaker used in the experiments.

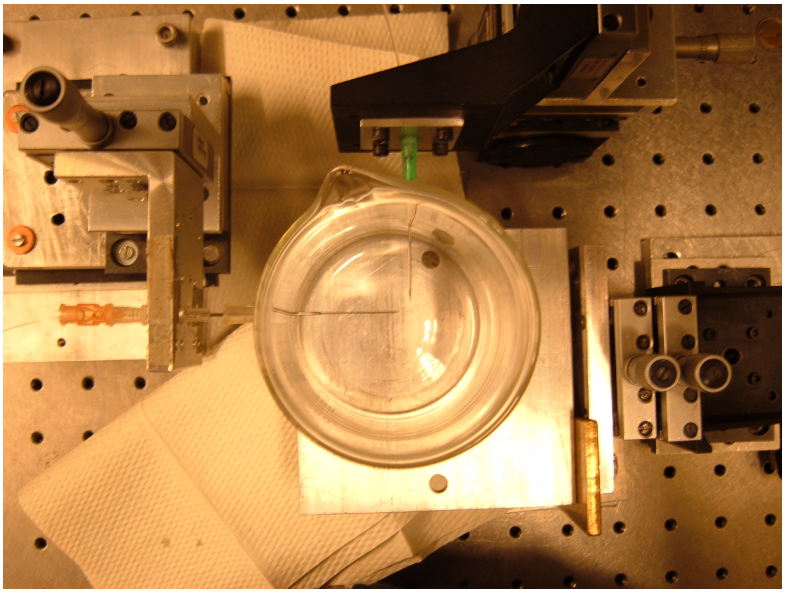

(b) Beaker in the sample holder.

Figure 8: Beaker used in the experiments.

the needle across several layers, when inserting needle along one layer and when extracting the needle along one layer. The samples were cut into suitable pieces, typically 6 cm by 6 cm and 2-4 cm thick. The reflectance and fluorescence of the salmon was measured. The spectra are found in the appendix.

Mass density of salmon
To calculate the absorption coefficient and the reduced scattering coefficient, the mass density of salmon is needed. The mass density used in this thesis, was found experimentally. The salmon was weighed, and put in a measuring cylinder containing a known amount of water. The new volume was read, and the difference in volumes equaled the space which was occupied by the salmon. The mass density found was 1.07±0.04g/mL, where 0.04 g/mL is the standard deviation. The weight used was Explorer Pro from Ohaus.

3.4 Assumptions in the coefficient calculations

3.4.1 Penetration depth

According to eq. (16) the natural logarithm to the fluence rate times distance, $\ln(\phi r)$, is proportional to the inverse of the penetration depth ,δ. The results from the measurements are plotted as $\ln(\phi r)$ as a function of r. By doing a linear fit it is possible to find the penetration depth. The linear fits were done by using the polyfit function in Matlab (Mathworks, v 7.50 R2007b).

3.4.2 The absorption coefficient of china ink

The absorbance of china ink has been found on an earlier occation by Randeberg et. al.[29]. The absorbance in the original data was found for a 2.75x10^{-2} vol.% ink solution. The absorbance is plotted in figure 9. The absorption coefficient was found from the equation, $\mu_{a,ink} = A/x$, where A is the absorbance and x is the thickness of the sample. The cuvettes used were 10 mm thick.

3.4.3 The reduced scattering coefficient of intralipid

The following assumptions were made; $\mu_{a,intralipid} << \mu_{a,ink}$ and $\mu'_{s,intralipid} >> \mu'_{s,ink}$. From these assumptions it is sufficient to use only one of the solution with intralipid and ink in the calculations. Solution 3 in table 7 was used in the calculation due to better accuracy in the volume of ink added. The reduced scattering coefficient of intralipid was found from the penetration depth of this solution, using eq. (13). The results from the measurements on solution 2 in table 7 are presented in the appendix.

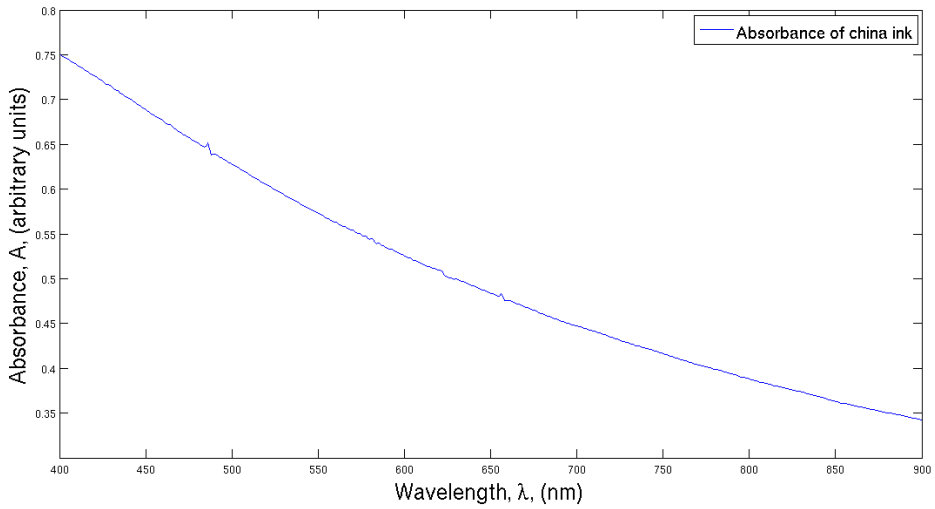

Figure 9: Absorbance of china ink as a function of wavelength. Average of three measurements.

3.4.4 The absorption coefficient and the reduced scattering coefficient of salmon

The following assumptions were made; $\mu_{a,intralipid} << \mu_{a,salmon}$ and $\mu'_{s,total} = D\mu'_{s,intralipid} + E\mu'_{s,salmon}$ (solution 4 in table 7), where D and E are the volume fraction of intralipid and salmon respectively. $D = 0.926$ and $E = 7.4 \cdot 10^{-2}$. In the calculations of the coefficients for the salmon, only the measurements from needle insertion were used.

3.4.5 Assumptions for the light scattering in the salmon

The transport mean free path had to be assumed before the measurements. In an earlier thesis[30] $l_{tr} = 5$ mm for salmon was assumed, and $l_{tr} = 3$ mm for a diluted solution of milk. Based on these l_{tr} and an educated guess, the l_{tr} in table 8 were assumed.

Table 8: Transport mean free path assumed in the measurements

Medium	l_{tr} (mm)
Intralipid	3
Intralipid and ink	3
Intralipid and mashed salmon	4
Salmon	5

3.5 Matlab code

Plotting and calculating were trivial for the measurements with the lasers, but the measurements with the halogen lamp produced huge amounts of data and needed a more thorough treatment. The data were organised as shown in figure 10. The description of the Matlab function, returnLimits.m, will be presented in this section. The description of other relevant Matlab functions made, are found in the appendix.

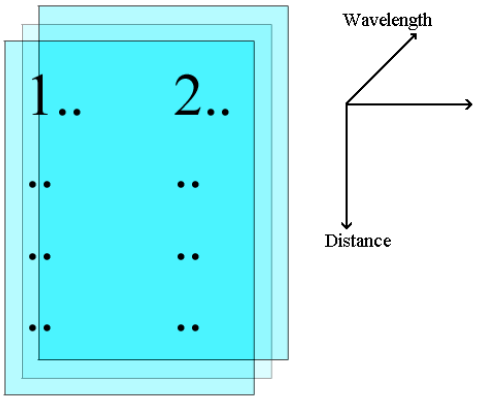

Figure 10: Illustration of the data stored in a 3-dimensional matrix

Matlab function, returnLimits.m

- Inputs; one 3-dimensional matrix, two integer values
- Outputs; none

This function handles all the limitations given, and returns the lower and upper wavelength, and the minimum and maximum distance to include in the linear fit. These limitations includes the number of points to use in the linear fit, a limitation regarding the signal to noise ratio (SNR) and a limit for when the spectrometer is considered saturated. One 3-dimensional matrix and two integers are entered. The 3-dimensional matrix corresponds to one of the measurements over all distances. The first integer entered is the number of points required in the linear fit. The second integer is the minimum distance (in mm) to include in the linear fit. The function changes this distance if the spectrometer was saturated. The distances used in the measurements are 5 mm to 20 mm. The background noise was defined as a certain number of photons per

integration time, which was found by studying selected measurements. It was assumed that there were no signal for the shorter wavelengths, and that the background noise was approximately equal for all wavelengths. An example is given in figure 11. This number was set to 200 photons per integration time. SNR = 3 was set as the limitation in the calculations, and no measurements with less than 600 photons per integration time were included. The limit for the saturation was set to 55000 photons per integration time.

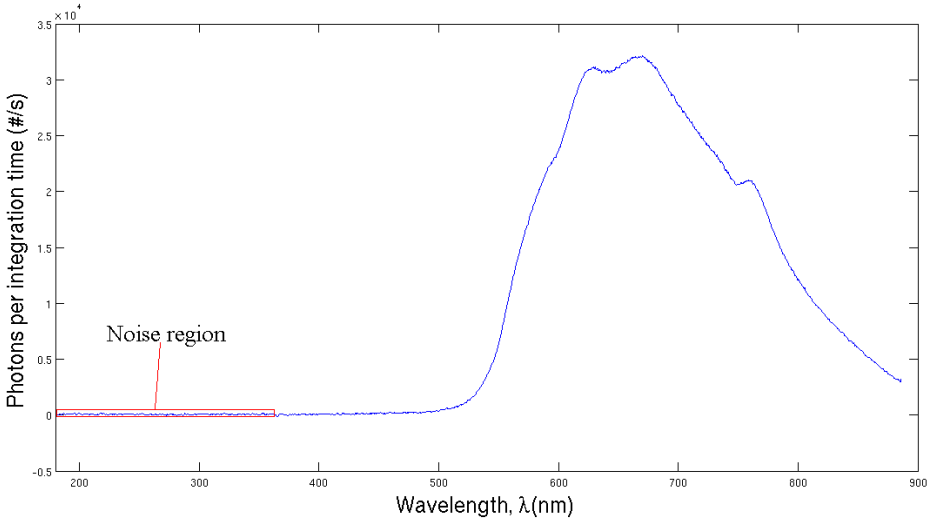

Figure 11: Photons per integration time as a function of wavelength, from the measurement across several layers for needle extraction. The distance from the center was 6 mm. The region of the curve ($\lambda < 360$nm) which was used to measure background noise is marked in the figure.

4 Results

4.1 Measurements with the lasers

The natural logarithm to the fluence rate times distance, $\ln(\phi r)$, is plotted as a function of distance, r, in the result for the lasers. The distances used in the linear fit are included in the table for the penetration depths. The penetration depth and the coefficients were found as described in section 3.4. The results from measurements with the YAG laser are plotted in figure 12-16. The penetration depths and the coefficients calculated from these measurements are shown in table 9 and table 10, respectively. The results from measurements with the He-Ne laser are plotted in figure 17-20. The penetration depths and the coefficients calculated from these measurements are shown in table 11 and table 12, respectively.

4.1.1 YAG laser

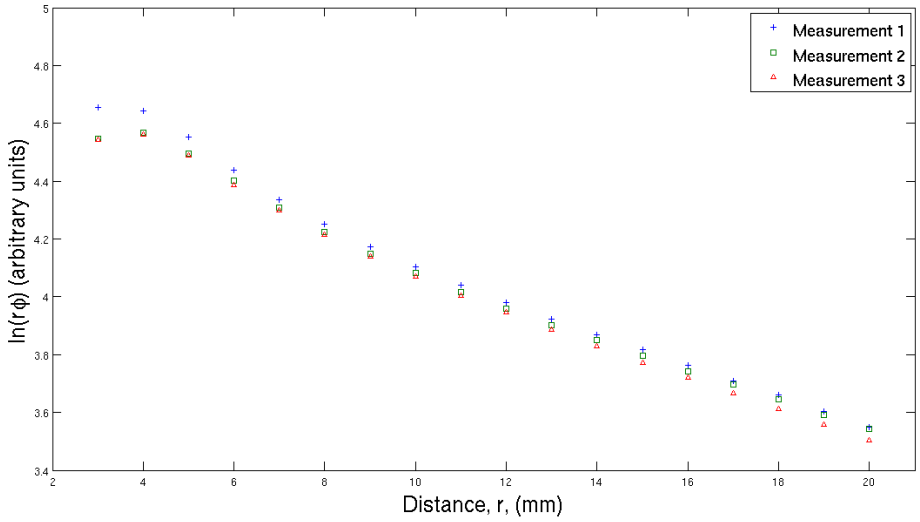

Figure 12: The natural logarithm to the distance times fluence rate, $\ln(r\phi)$, as a function of distance, r, for intralipid. Three measurements were performed. Light source: YAG laser.

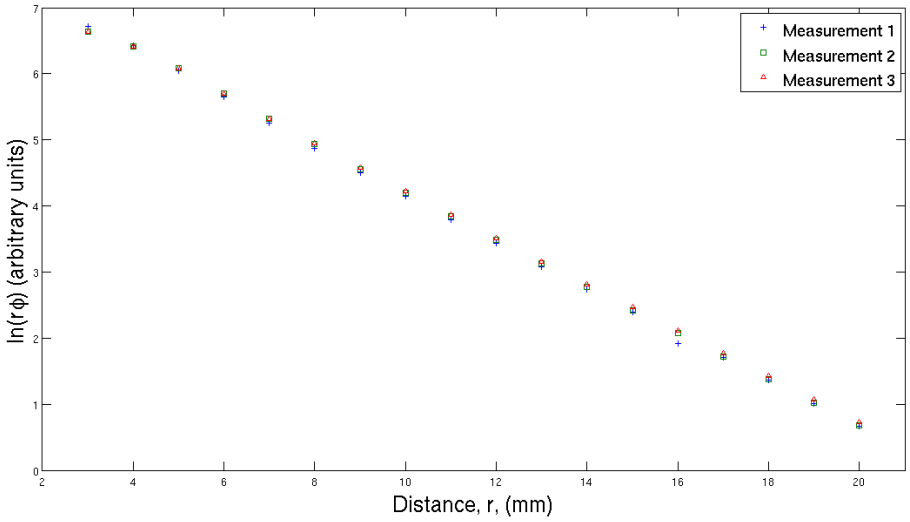

Figure 13: The natural logarithm to the distance times fluence rate, $\ln(r\phi)$, as a function of distance, r, for the mixture of ink and intralipid. Three measurements were performed. Light source: YAG laser.

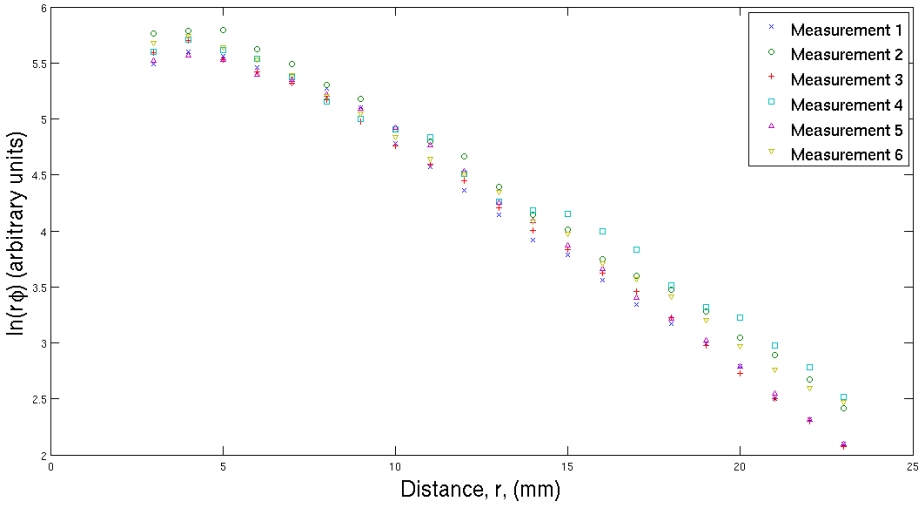

Figure 14: The natural logarithm to the distance times fluence rate, $\ln(r\phi)$, as a function of distance, r, for the mixture of mashed salmon and intralipid. Six measurements were performed. Light source: YAG laser.

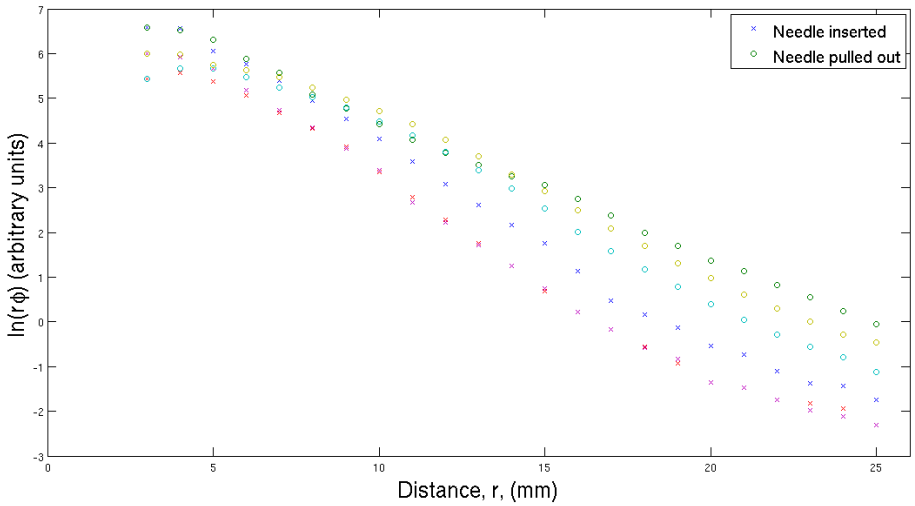

Figure 15: The natural logarithm to the distance times fluence rate, $\ln(r\phi)$, as a function of distance, r, for measurements across several layers in the salmon. Three measurements were performed. Light source: YAG laser.

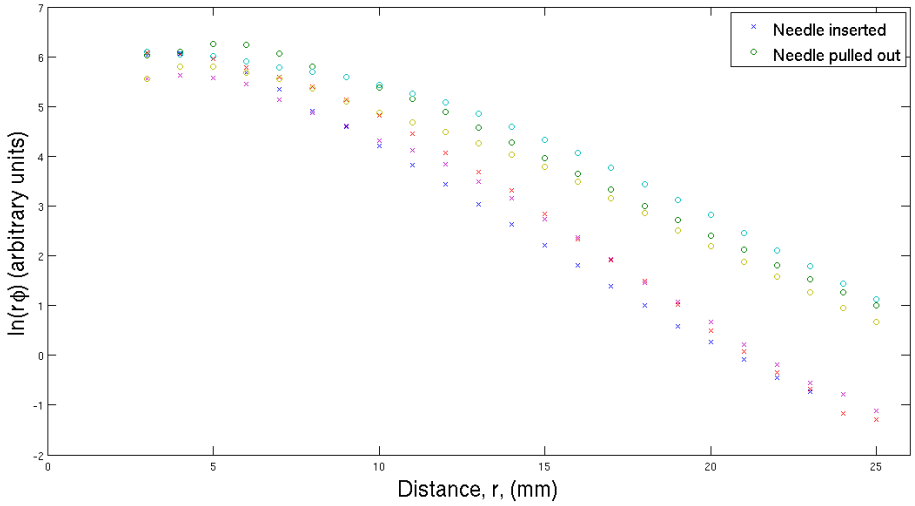

Figure 16: The natural logarithm to the distance times fluence rate, $\ln(r\phi)$, as a function of distance, r, for measurements along one layer in the salmon. Three measurements were performed. Light source: YAG laser.

Table 9: Penetration depths for the YAG laser

	Needle inserted/ extracted	Penetration depth (mm)	Distances used in the linear fit (mm)
Intralipid	-	16.31±0.25	6-20
Intralipid and Ink	-	2.81±0.02	6-20
Intralipid and mashed salmon	-	5.21±0.42	7-23
Across layers in the salmon	in	2.08±0.03	6-20
Across layers in the salmon	out	2.93±0.27	6-20
Along one layer in the salmon	in	2.73±0.25	6-20
Along one layer in the salmon	out	4.14±0.51	6-20

Table 10: The absorption coefficients and the reduced scattering coefficients obtained from the measurements with the YAG laser.

	μ_a m^{-1}	μ_s' m^{-1}
China ink	26.94	0
Intralipid	0.814	1539
Salmon, along one layer	114	237
Salmon, across several layers	112	558

4.1.2 He-Ne laser

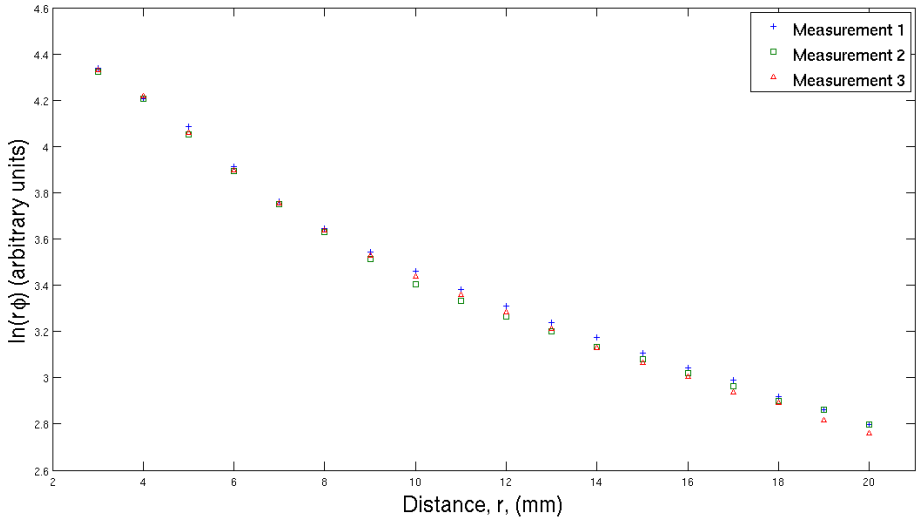

Figure 17: The natural logarithm to the distance times fluence rate, $\ln(r\phi)$, as a function of distance, r, for intralipid. Three measurements were performed. Light source: He-Ne laser.

Table 11: Penetration depths for the He-Ne laser

	Needle inserted/ extracted	Penetration depth (mm)	Distances used in the linear fit (mm)
Intralipid	-	12.96±0.32	6-20
Intralipid and Ink	-	3.32±0.05	6-20
Across layers in the salmon	in	6.79±0.33	8-25
Across layers in the salmon	out	8.43±1.49	10-25
Along one layer in the salmon	in	10.76±1.03	7-25
Along one layer in the salmon	out	10.80±0.45	11-25

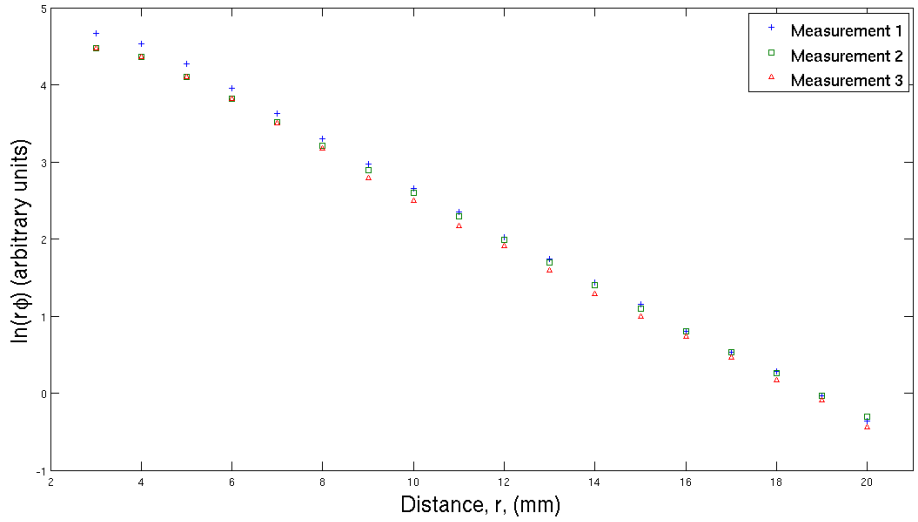

Figure 18: The natural logarithm to the distance times fluence rate, $\ln(r\phi)$, as a function of distance, r, for the mixture of ink and intralipid. Three measurements were performed. Light source: He-Ne laser.

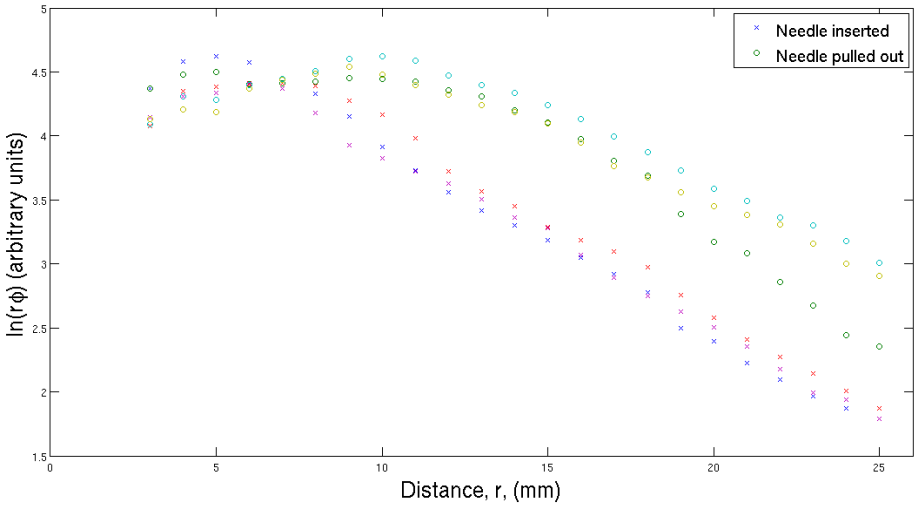

Figure 19: The natural logarithm to the distance times fluence rate, $\ln(r\phi)$, as a function of distance, r, for measurements across several layers in the salmon. Three measurements were performed. Light source: He-Ne laser.

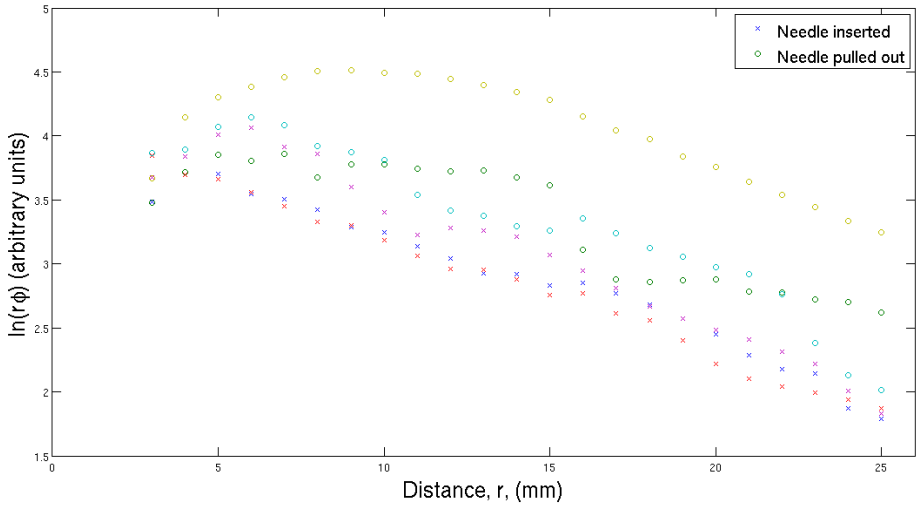

Figure 20: The natural logarithm to the distance times fluence rate, $\ln(r\phi)$, as a function of distance, r, for measurements along one layer in the salmon. Three measurements were performed. Light source: He-Ne laser.

Table 12: The absorption coefficients and the reduced scattering coefficients obtained from the measurements with the He-Ne laser.

	μ_a m^{-1}	μ_s' m^{-1}
China ink	22.65	0
Intralipid	1.510	1313

4.2 Halogen lamp and spectrometer

The penetration depth and the coefficients are plotted as a function of wavelength. The results from the lasers are included in the plot for all penetration depths, and for the coefficients to the intralipid. The vertical lines in these plots represents the wavelengths of the lasers, and the "x" mark the results obtained from measurements with the lasers. In all plots for the penetration depth the blue upper curve is the average calculated penetration depth, and the black lower curve is one standard deviation. The penetration depths and the coefficients were calculated as described in section 3.4. The distances used in the linear fit are shown in table 13.

Table 13: Distances used in the linear fit

	Distances used in the linear fit (mm)
Intralipid	8-15
Intralipid and ink	10-13
Intralipid and mashed salmon	10-15
Needle inserted into the salmon	6-11
Needle extracted from the salmon	10-16

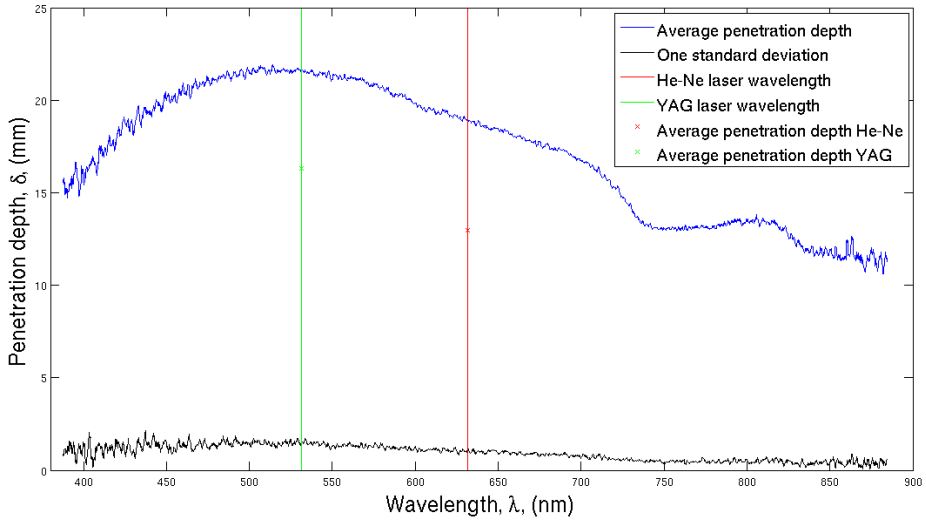

Figure 21: The penetration depth, δ, as a function of wavelength, λ, for intralipid. The blue upper curve is the average of the meaurements, while the lower black curve is the standard deviation of the measurements. The vertical lines and the "x" represent the wavelength and the result from the He-Ne laser and the Yag laser. Three measurements were performed. Light source: Halogen lamp.

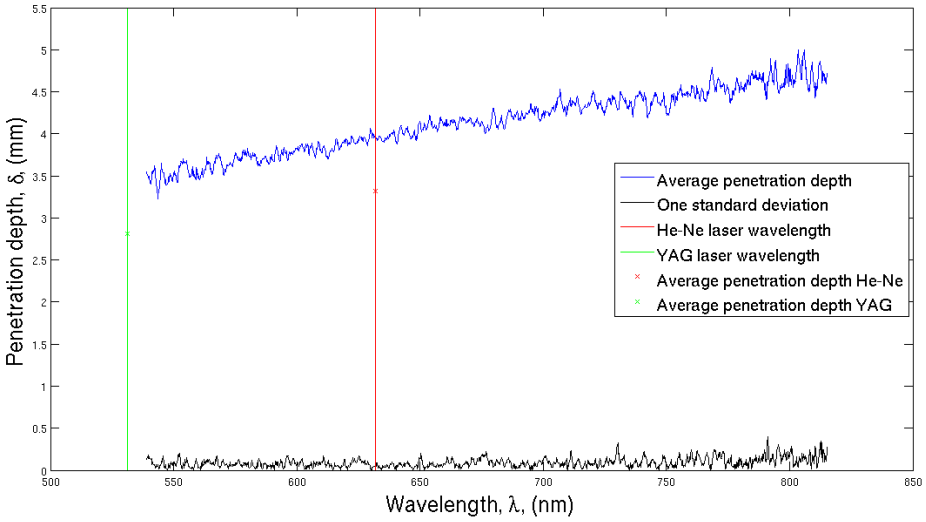

Figure 22: The penetration depth, δ, as a function of wavelength, λ, for the mixture of ink and intralipid. The blue upper curve is the average of the meaurements, while the lower black curve is the standard deviation of the measurements. The vertical lines and the "x" represent the wavelength and the result from the He-Ne laser and the Yag laser. Three measurements were performed. Light source: Halogen lamp.

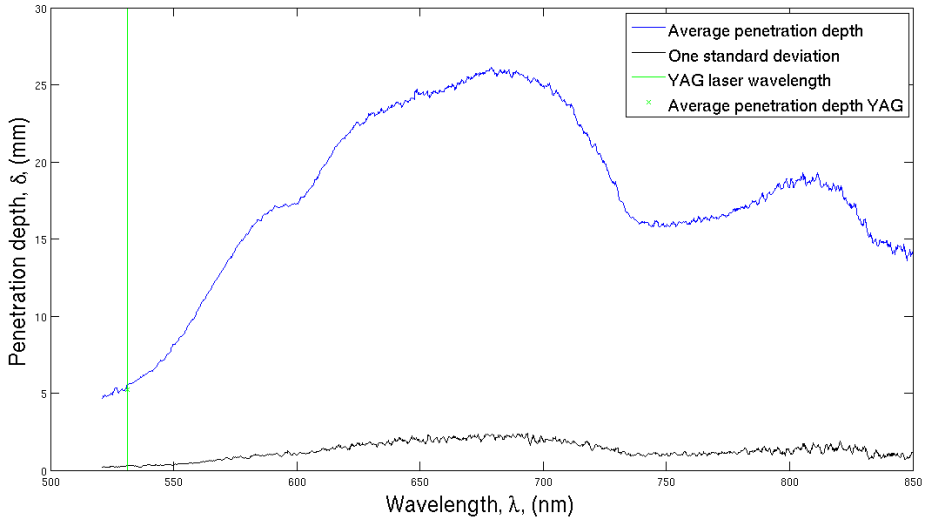

Figure 23: The penetration depth, δ, as a function of wavelength, λ, for the mixture of mashed salmon and intralipid. The blue upper curve is the average of the meaurements, while the black lower curve is the standard deviation of the measurements. The vertical line and "x" represents the wavelength and the result from the Yag laser. Six measurements were performed. Light source: Halogen lamp.

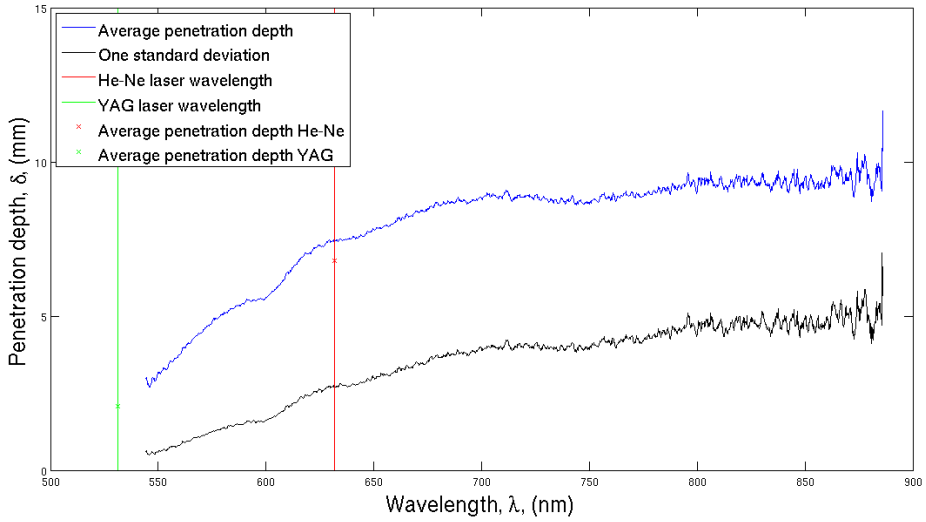

Figure 24: The penetration depth, δ, as a function of wavelength, λ, for needle insertion across several layers in the salmon. The blue upper curve is the average of the meaurements, while the black lower curve is the standard deviation of the measurements. The vertical lines and the "x" represent the wavelength and the result from the He-Ne laser and the Yag laser. Three measurements were performed. Light source: Halogen lamp.

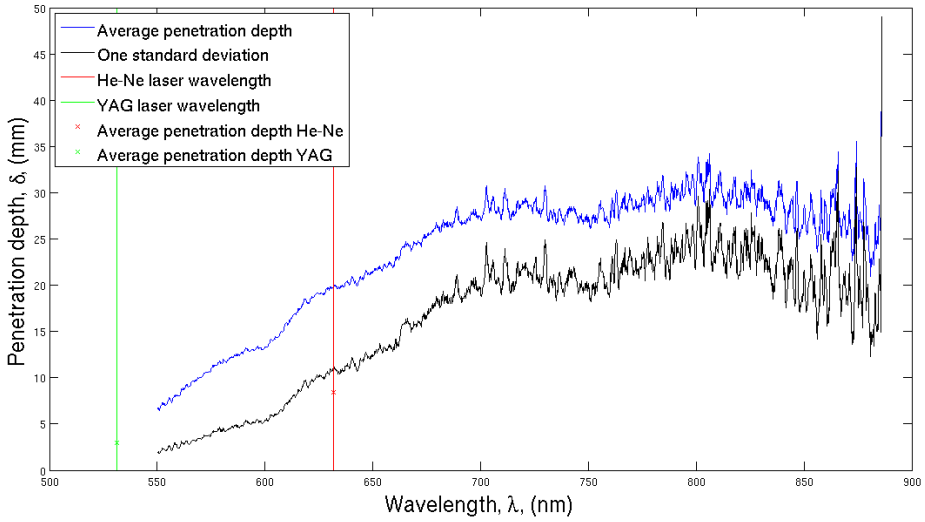

Figure 25: The penetration depth, δ, as a function of wavelength, λ, for needle extraction across several layers in the salmon. The blue upper curve is the average of the meaurements, while the black lower curve is the standard deviation of the measurements. The vertical lines and the "x" represent the wavelength and the result from the He-Ne laser and the Yag laser. Three measurements were performed. Light source: Halogen lamp.

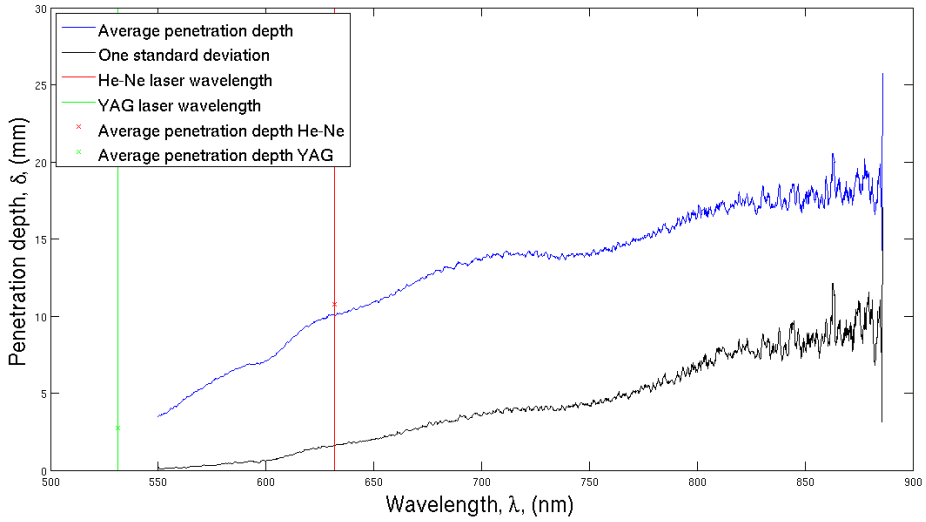

Figure 26: The penetration depth, δ, as a function of wavelength, λ, for needle insertion along one layer in the salmon. The blue upper curve is the average of the meaurements, while the black lower curve is the standard deviation of the measurements. The vertical lines and the "x" represent the wavelength and the result from the He-Ne laser and the Yag laser. Three measurements were performed. Light source: Halogen lamp.

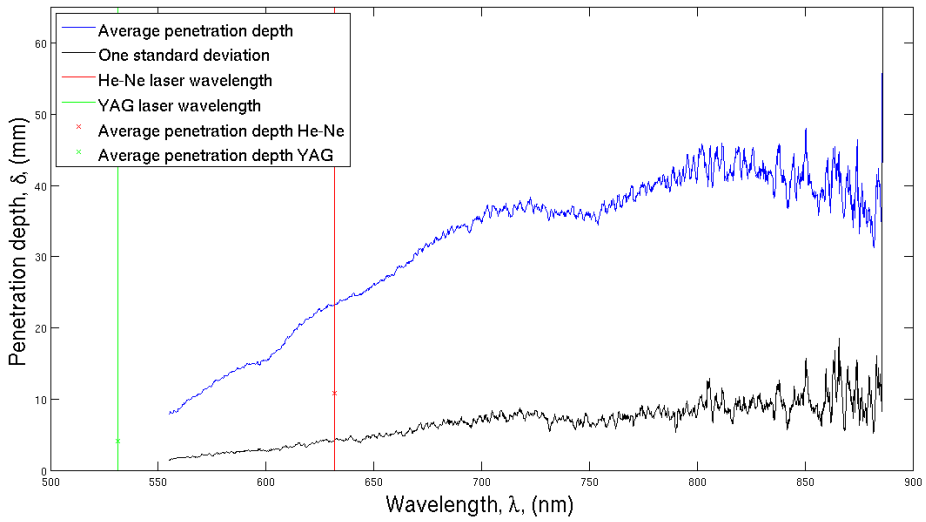

Figure 27: The penetration depth, δ, as a function of wavelength, λ, for needle extraction along one layer in the salmon. The blue upper curve is the average of the meaurements, while the black lower curve is the standard deviation of the measurements. The vertical lines and the "x" represent the wavelength and the result from the He-Ne laser and the Yag laser. Three measurements were performed. Light source: Halogen lamp.

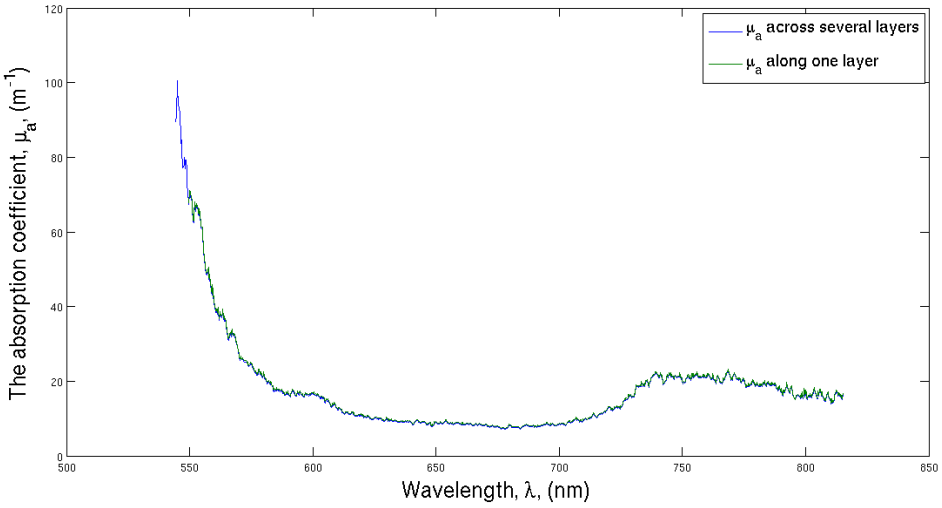

Figure 28: The absorption coefficient, μ_a, as a function of wavelength, λ, for measurements along one layer and across several layers. Light source: Halogen lamp.

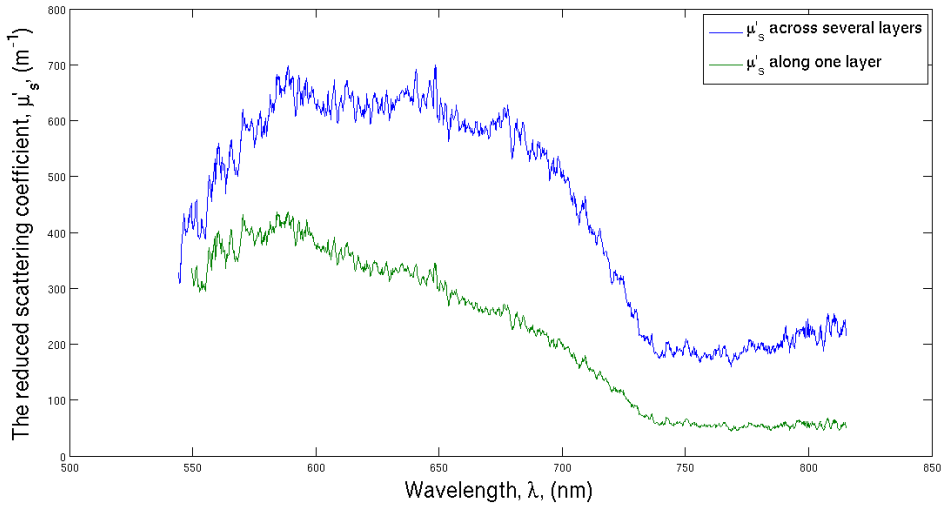

Figure 29: The reduced scattering coefficient, μ_s', as a function of wavelength, λ, for measurements along one layer and across several layers. The green lower curve is from measuring along one layer. The blue upper curve is from measuring across several layers. Light source: Halogen lamp.

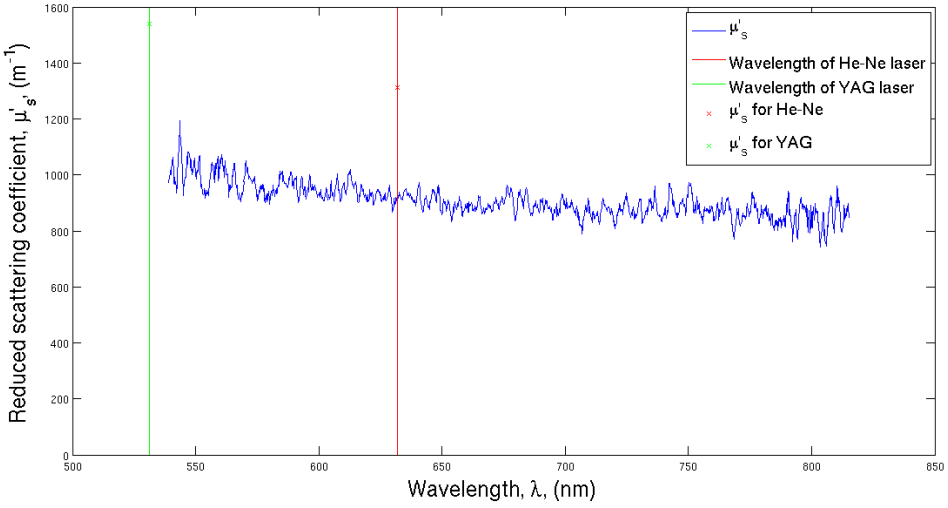

Figure 30: The reduced scattering coefficient, μ_s', as a function of wavelength, λ, for intralipid. The average penetration depth was used in the calculations. The vertical lines and the "x" represent the wavelength and the result from the He-Ne laser and the Yag laser.

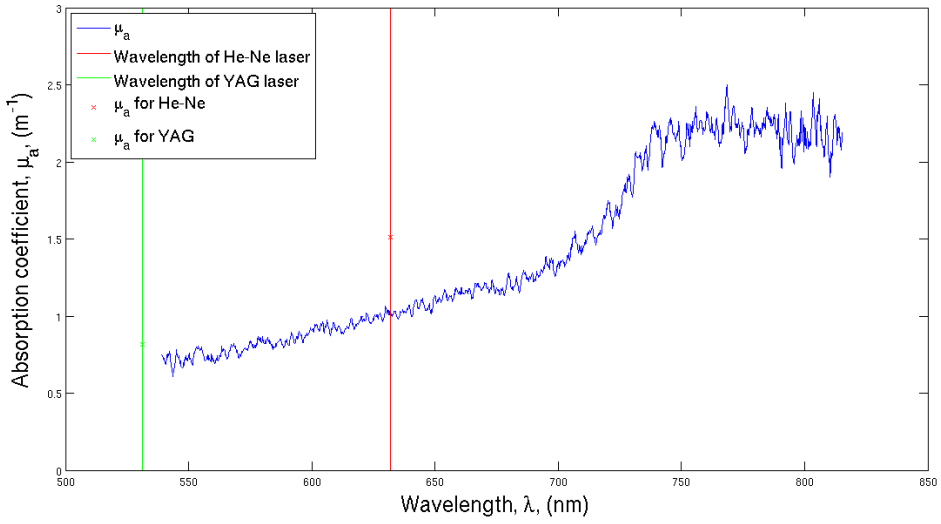

Figure 31: The absorption coefficient, μ_a, as a function of wavelength, λ, for intralipid. The average penetration depth was used in the calculations. The vertical lines and the "x" represent the wavelength and the result from the He-Ne laser and the Yag laser.

5 Discussion

5.1 Results, intralipid

The measurements on the fluids yielded little variation in the results. This was expected, due to the approximations done. The fluids are closer to a homogenous medium, and the accuracy in concentration when adding constituents is good. In the literature the coefficients of intralipid are often given for a 10-% intralipid solution[31][32][33]. That means that the intralipid contains 10 g of lipid per 100 mL.

The reduced scattering coefficient
It was assumed that the reduced scattering coefficient of intralipid was much larger than the reduced scattering coefficient of any other substance in the solution. It was also assumed that the reduced scattering coefficient for a 10-% intralipid solution may be found by a scaling factor (based on the measurements on a diluted intralipid solution). The reduced scattering coefficient for a 10-% intralipid solution found in this thesis is plotted in figure 32, and the result from the measurement with the He-Ne laser is found in table 12. Moes et al.[31] found $\mu'_{s,intralipid} = 11190 \pm 120$ m^{-1} at $\lambda = 633$ nm (calculated from the μ_s and the anisotropy factor found). Van Stavern et al.[32] found $\mu'_{s,intralipid} = 9710$ m^{-1} at $\lambda = 632.8$ nm (calculated from the μ_s and the anisotropy factor found). μ'_s found in this thesis was about four to five times larger. The reduced scattering coefficient was also compared with those found by Michels et al.[33]. The scattering coefficient presented in this thesis was found to be two to four times larger. The reduced scattering coefficient found in this thesis is larger than expected compared to what is found in the literature. This may be due to the assumption made in the calculation of μ'_s for a intralipid 10-% solution. The optical properties of the fat emulsion may vary much for the same brand[33], meaning that different order of intralipid may have different optical properties. A combination of the above may explain the large deviation in the comparison.

The absorption coefficient
The absorption coefficient of intralipid, solution 1 in table 7, is plotted in figure 31. This solution consisted of tap water and intralipid. Pope et al.[34] found the absorption coefficient for pure water in the visible wavelengths. The water contributes to more than 20 % of the total absorption coefficient for 600nm $< \lambda <$ 730nm. At $\lambda = 720$nm, the water contributes to about 70 % of the total absorption. If the absorption coefficient of intralipid is to be found, one needs to correct for the absorption from water. This was not done in this thesis, as the focus was to find the optical properties in salmon.

5.2 Results, salmon

The measurement on the mixture of mashed salmon and intralipid was carried out only for the YAG laser and the halogen lamp. For the YAG laser this measurement was disregarded due to a large uncertainty. This uncertainty is discussed in section 5.3.3.

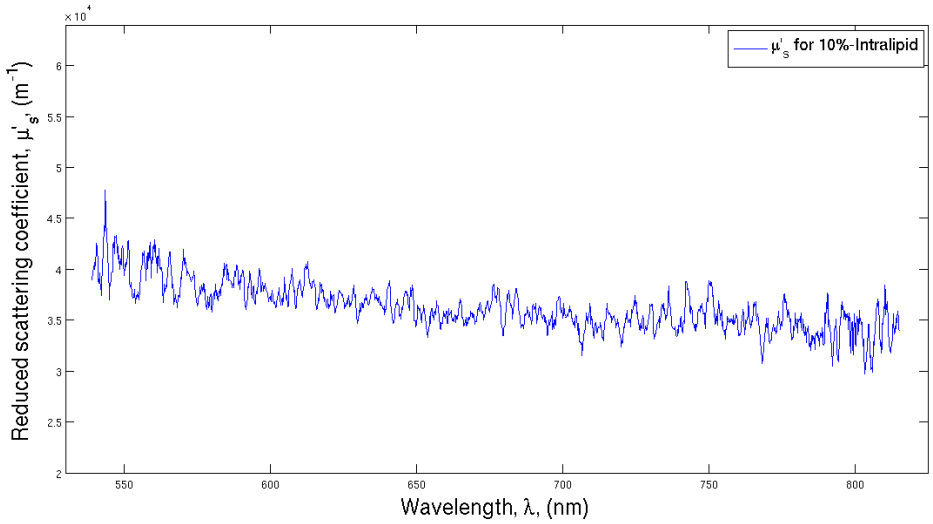

Figure 32: The reduced scattering coefficient, μ_s', as a function of wavelength, λ, for a 10-% intralipid solution.

Only the penetration depth obtained from the measurement with the lasers may be compared with the result from the halogen lamp.

5.2.1 Needle insertion versus needle extraction

A significant difference in the results was found dependent on whether the needle was inserted or extracted of the salmon. When the needle was extracted, the fluence rate decreased significantly less the first millimeters. This lead to a difference in the distances chosen for the linear fit. The penetration depths found were significantly larger for when the needle was extracted, on average the penetration depth found was 45% larger for the lasers. This is based on the penetration depths given in table 9 and 11. From measuring across several layers with the halogen lamp, the penetration depth found was 190% larger on average for needle extraction. From measuring along one layer with the halogen lamp, the penetration depth found was 140% larger on average for needle extraction. The difference is probably due to the canal made by the needle. From what was seen from the outside, the canal did not collapse after extracting the needle. It is likely that the canal was filled with either air or fat from the salmon. In either cases both air and fat are more translucent than the salmon, yielding a larger penetration depth. Due to this error, the calculation of μ_a and μ_s' are based on the measurements from inserting the needle.

5.2.2 Measurements across several layers versus measurements along one layer

The measurements showed a significant difference in the penetration depth. For measurements with the lasers, the penetration depth found was 38% larger on average for measurements along one layer compared to the measurements across several layers. This is based on the penetration depths given in table 9 and 11. For needle insertion measurements with the halogen lamp, the penetration depth found was 57% larger on average for measurements along one layer. For needle extraction measurements with the halogen lamp, the penetration depth found was 30% larger on average for mesurements along one layer.

For the halogen lamp μ_a and μ_s' were found. Two different results were obtained by using both the measurements from inserting the needle (across severeal layers and along one layer). Figure 33 is a simplified illustration of the salmon. Assume that the center point (isotropic source) is in point A, and that the detector fiber is kept in either point B or C. Measuring across several layers corresponds to measuring the photons transported from A to B. Measuring along one layer corresponds to measuring the photons transported from A to C. Assuming that the membrane between the layers in the salmon has a different refractive index than the muscle tissue gives a Fresnel reflection at these boundaries. The arrows represents the net flow of photons. From the illustration it is possible to see that the Fresnel reflection gives a net negative contribution (back scattering) to g when measuring across several layers. When measuring along one layer the Fresnel reflections gives a net positive contribution (forward scattering) to g. This suggests a lower μ_s', and a larger penetration depth for measurements along one layer.

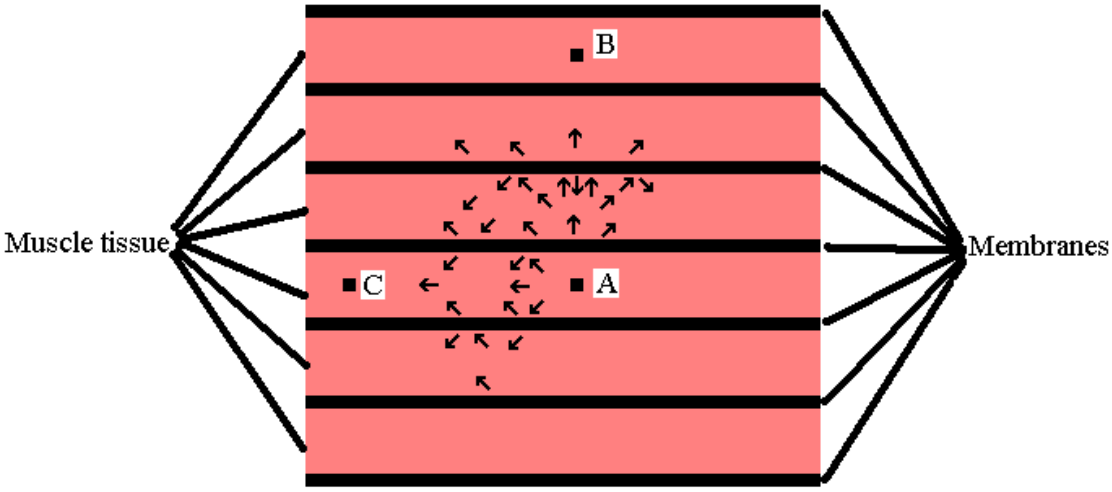

Figure 33: Illustration of possible Fresnel reflections in the salmon.

μ_a is plotted in figure 28, and μ_s' is plotted in figure 29. As shown in figure 28, no significant differences in μ_a were found. In figure 29, significant differences in μ_s' were found,

μ_s' along one layer was smaller than μ_s' across several layers for all wavelengths. The results from the measurements with the lasers showed a significantly larger penetration depth for the measurements along one layer. This is in accordance with the presented hypothesis, and may therefore be an explanation to the differences obtained from the measurements along one layer compared to the measurements across several layers. The uncertainty in the measurements on salmon may not explain such a systematic difference in the results.

5.2.3 Comparing the measurements with lasers to the measurement with the halogen lamp

The results from the He-Ne laser and the YAG laser were included in the plots for the halogen lamp, see figure 21-27 and figure 30-31. μ_a and μ_s' found for the salmon with the YAG laser were not reliable due to the formation of lumps in the solution of mashed salmon and intralipid. This will be discussed in section 5.3.3. The wavelength of the YAG laser was close to the lowest wavelength included in the results from the halogen lamp, and was included in the plots. From assuming how the curve would develope towards the wavelength of the YAG laser it was possible to do a comparison. μ_s' and μ_a for intralipid, and all the penetration depths obtained from the measurements with the lasers is compared to the results obtained from the measurements with the halogen lamp.

Comparison of the results from measurements on fluids
The standard deviation in the measurements with the halogen lamp is small, but still larger than those obtained with the lasers. The penetration depths from measurements with the halogen lamp were significantly larger, figure 21 and 22. Results from the mixture of mashed salmon and intralipid agreed. This was considered a coincidence due to the high uncertainty in the measurements with the YAG laser. The larger penetration depths found, lead to smaller μ_a and μ_s' in the calculations based on the results from the halogen lamp. These results suggests a systematic error (e.g. the response curve in the detectors or in the calculations).

Comparison of the results from measurements on salmon
The standard deviation in the measurements with the halogen lamp is larger. From needle insertion the measurements are in correspondence with those obtained with the lasers, considering the large variation in the results. From needle extraction the penetration depths were about twice as large for the halogen lamp compared to the results from the He-Ne laser. It seemed to be more in correspondence to the results obtained from the YAG laser. In section 5.2.1 it was concluded that the measurements from needle extraction yielded inconsistent results. Based on the measurements from needle insertion the results agrees well. The standard deviation in the results obtained from the measurements with the halogen lamp is large, and the results are uncertain. It will

be difficult to reproduce the results obtained from the halogen lamp.

5.2.4 Comparison with literature

Measurements on salmon have been performed in an earlier thesis[30]. The penetration depth was found for fresh salmon, and defrosted salmon at $\lambda = 488$ nm and $\lambda = 655$ nm. No results for $\lambda = 488$ nm were obtained in this thesis, and only the results for $\lambda = 655$ nm obtained from the measurements with the halogen lamp are compared. The comparison is shown in table 14. In the comparison the average of the penetration depth found from measuring along one layer and measuring across several layers for needle insertion are used. This is due to unknown facts about whether the measurements were made along one layer or across several layers in the compared results. The penetration depth in salmon found in this thesis is smaller. This may be explained by the possible variation in the optical properties in salmon. The optical properties will probably be dependent on the location on the salmon of which the measurements are performed, and between individual fish. Variations may also be caused by the process of smoking the salmon. Smoking the salmon causes weight loss in the salmon[35], which alters the concentration of e.g. astaxanthin and fat. The optical properties are dependent on the concentrations of absorbing and scattering particles, and a change in the penetration depth is expected.

Table 14: Penetration depth of salmon

	Wavelength (nm)	Penetration depth (mm)	Reference
Unprocessed salmon	655	10.7±2.3	[30]
Defrosted salmon	655	13.8±1.9	[30]
Smoked salmon, across several layers	655	7.9±3.1	Figure 24
Smoked salmon, along one layer	655	11.2±2.2	Figure 26

5.3 Potential sources of error

5.3.1 Uncertainty in the calculations

Linear fit

The linear fit has to be carried out in the linear region (with a slope) of the curve. This is where the validity of the diffusion approximation is best. In the measurements with the lasers, it was easy to pick an applicable region. However, in the measurements with the halogen lamp, it was not possible to study the plots for every wavelength. The distances included in the linear fit were decided based on studying plots for selected wavelengths. This may have lead to some error in the results for the halogen lamp.

In the measurements with the halogen lamp, it was difficult to decide the number of points to include in the linear fit. If more points are included in the linear fit, the result

will be less vulnerable to single points deviating from the linear curve. If less points are included in the linear fit, the wavelength range for which the results are plotted would be larger. In this thesis the number of points included in the linear fit were a compromise based on these issues. In the lowest wavelengths included in the results from the halogen lamp, measurements with SNR≈3 are included in the linear fit. The low SNR may affect the result significantly for these wavelengths. The linear fit itself is uncertain. Variations in the distances included in the fit will affect the result. There is no single correct answer for which distances should be included in the linear fit, and the result will depend on the data analysis. However, if the linear region of the curve is chosen there will not be too large variations. Table 15 shows the results for the He-Ne laser by including different distances (from the linear region) in the linear fit for needle insertion across several layers, see figure 19.

Table 15: Penetration depths for the He-Ne laser for needle insertion across several layers with small variations in the distances included in the linear fit, see figure 19.

Penetration depth (mm)	Distances used in the linear fit (mm)
6.79±0.33	8-25, used in the calculations
6.87±0.39	7-20
6.81±0.38	7-22
6.80±0.28	7-25
6.86±0.48	8-20
6.80±0.46	8-22

The validity of the diffusion approximation

The diffusion approximation involves many assumptions. Among others, an infinite medium was assumed and no inelasitc scattering was assumed. None of the samples in this thesis were an infinite medium, and this may have affected the results. The salmon does show fluorescence, hence the assumption of no inelastic scattering is not entirely correct. The fluorescence is significant for $\lambda < 600$nm in the salmon, but most of the fluorescent photons will probably be reabsorbed due to the presence of astaxanthin. If the intralipid is fluorescent, it may have affected the measurements on the fluids.

In section 2.3 $\mu_a << \mu_s'$ was stated as a criterion for the validity of the diffusion approximation. In figure 34 μ_s'/μ_a is plotted as a function of wavelength for the measurements along one layer and across several layers in the salmon. The red dashed line corresponds to $\mu_s' = 10\mu_a$, which should be the minimum requirement for claiming the diffusion approximation as a good approximation. Based on this requirement the validity of the diffusion approximation is fair for $\lambda > 570$ nm when measuring across several layers. The results from measuring along one layer yielded a smaller μ_s'/μ_a, and the

penetration depths in salmon measured with the halogen lamp have very large standard deviations. This means that the diffusion approximation may be poor even if $\mu_s' = 10\mu_a$, and the requirement should be stricter. μ_s'/μ_a is considerably larger than the minimum requirement for wavelengths from about 600 nm up to about 700 nm in the results from measurements both along one layer and across several layers. The diffusion approximation is probably a good approximation for wavelengths in this interval. The results from intralipid yields $\mu_s'/\mu_a > 100$ for all wavelengths studied in this thesis and the diffusion approximation is probably a good approximation for measurements on intralipid. μ_s' and μ_a in intralipid are plotted in figure 30 and figure 31.

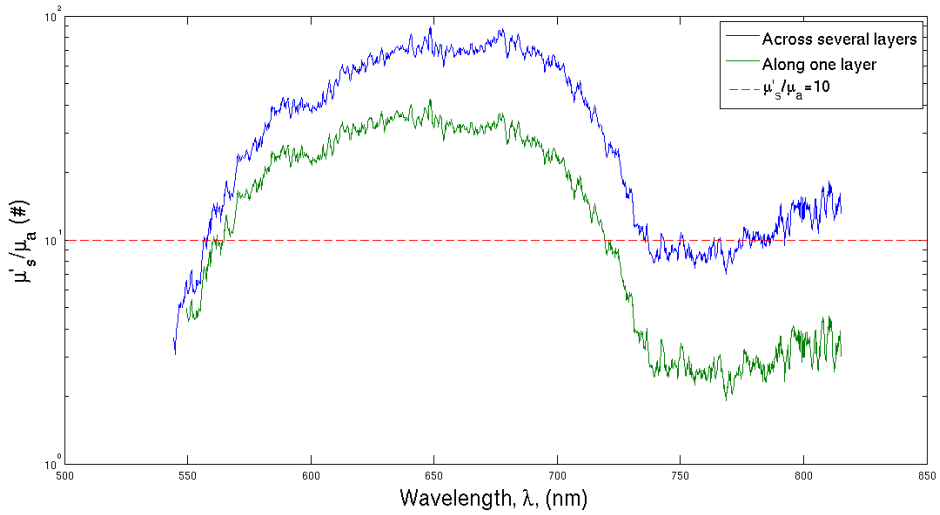

Figure 34: The reduced scattering coefficient divided by the absorption coefficient, μ_s'/μ_a, as a function of wavelength, λ, for the measurements along one layer and across several layers in the salmon.

5.3.2 Uncertainty in the measurements

Transport mean free path

The transport mean free path was found from eq. 4. Table 16 summarizes the assumed transport mean free path, and the ones calculated from the results. The calculation of the transport mean free path for the mixture of mashed salmon and intralipid was based on the coefficients obtained from measuring across several layers in the salmon.

Table 16 shows that the transport mean free paths assumed were too large. The shift of the detector fiber with respect to the center point does affect the measurements for small distances. The true distance measured is a bit larger than the assumed distance. This is illustrated in figure 35. In figure 36 the transport mean free path is plotted as a function of wavelength for salmon from measuring across several layers. The dashed line indicates the transport mean free path assumed in the measurements.

Table 16: Transport mean free paths

	Wavelength (nm)	l_{tr} assumed in the experiments (mm)	l_{tr} calculated from the results (mm)
Intralipid	631.79	3	0.76
Intralipid and ink	631.79	3	0.75
Salmon across several layers	631.79	5	-
Salmon along one layer	631.79	5	-
Intralipid	531.24	3	0.65
Intralipid and ink	531.24	3	0.64
Mashed salmon and intralipid	531.24	4	0.68
Salmon across several layers	531.24	5	1.49
Salmon along one layer	531.24	5	2.85

The assumed transport mean free path and the experimentally found transport mean free path matched well for $\lambda > 730$ nm. The corresponding plot from measuring along one layer yields a larger transport mean free path due to the smaller μ_s'.

Salmon
The measurements were done over a time span of weeks. It was unrealistic to do all the measurements on the same salmon. However, all the measurements for each individual light source were done on the same salmon. The optical properties may vary dependening on the location on the salmon (due to the distribution of fat and astaxanthin), and between individual fishes (due to the content of fat and astaxanthin). Most of the salmons were bought in fillets, and the exact location on the salmon were unknown. This may have lead to variation in the results between the lasers and the halogen lamp.

The needle was inserted into the salmon according to the orientation of the layers at the surface. If one wants to make sure that the needle really was inserted along one layer, it is possible to do a destructive analysis after the measurements. The destructive analysis consists of removing the flesh above the needle while the needle is still inserted. Measurements were done pulling the needle out of the salmon in the same canal that was made inserting the needle. This is incompatible with the destructive analysis, hence the destructive analysis was not carried out.

5.3.3 Potential sources of error in the measurements

The length of the fiber outside the tip of the needle was about 0.5 mm. This is significantly shorter than the penetration depths found, and reflections from the needle may have affected the amount of light coupled into the detector fiber. This distance was only changed between the measurements with the halogen lamp and the lasers. The

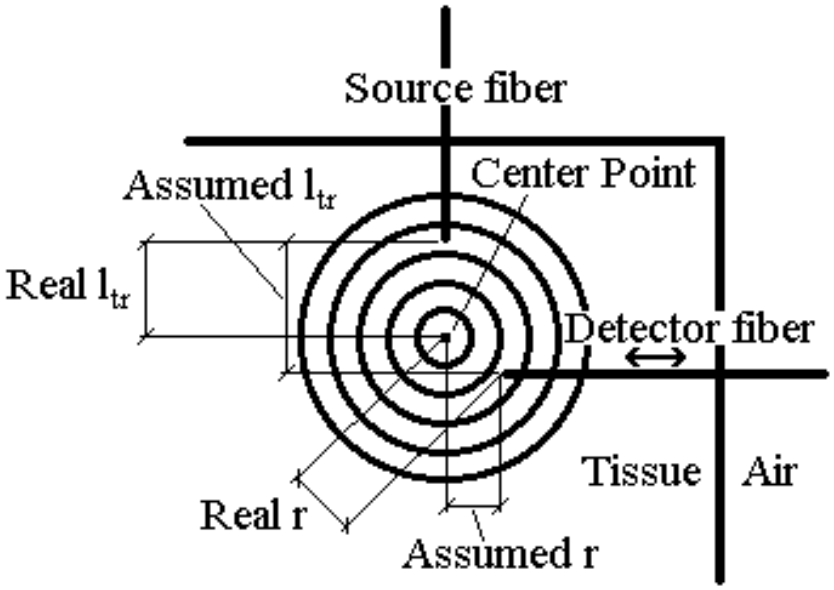

Figure 35: Assuming too large transport mean free path.

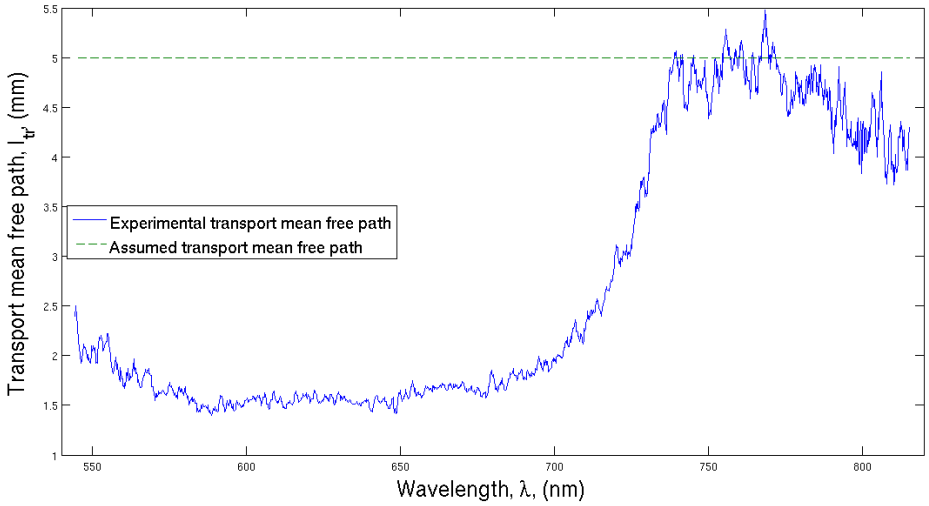

Figure 36: The transport mean free path, l_{tr}, as a function of wavelength, λ, for measurements across several layers in the salmon. The experimentally transport mean free path was calculated from the coefficients obtained from the measurements across several layers, figure 28 and 29. The dashed line indicates the assumed transport mean free path in the measurements.

reflections may have introduced some errors to the results.

When measurements were done close to the boundary between two layers in the salmon, the validity of the diffusion approximation is limited. This may have lead to single points deviating from the linear behaviour of the curve.

The fiber is not perfectly fitted into a needle, hence there will be a gap between the fiber and the needle. During the measurements on the salmon, strips of tissue and fat was wedged in this gap. These strips were removed before each new insertion in the salmon. Making the measurement over again was not an option due to the frequent occurence of this phenomenon. These strips may have affected the amount of light coupled into the detector fiber.

Solution 4 in table 7 was mixed by a handblender. During the measurements with the YAG laser, lumps were formed. The lumps sank to the bottom of the glass leaving a more transparent fluid at the top. This did affect the measurement significantly. With the halogen lamp no lumps were seen immediately after the measurements. This may be due to the fresher intralipid used. The lumps dispersed when the mixture was stired. Using a magnet mixer may solve this problem, but the currents created will perhaps affect the measurements. Replacing the intralipid with milk (throughout the experiments) as the scattering fluid may be a solution to the problem of formation of lumps. Milk has earlier been used as the scattering fluid in similar experiments[29].

During the measurements on the fluids, a leakage was noticed. This leakage was through the needle inserted in the beaker, illustrated in figure 37. The size of the leakage was small compared to the duration of one measurement. This may have lead to a small variations in the results.

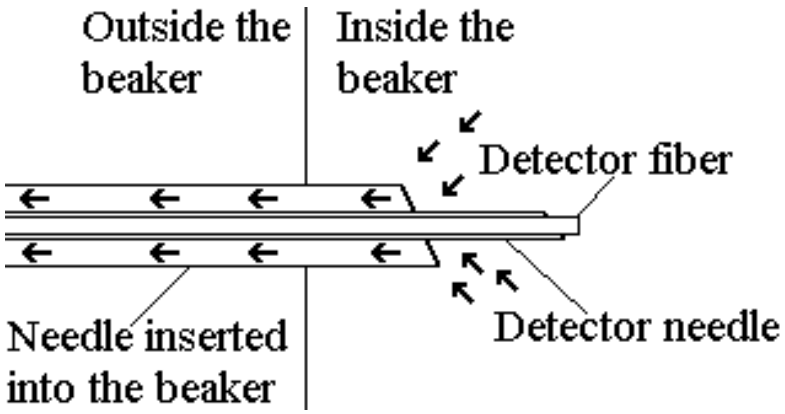

Figure 37: Leakage through the needle in the beaker. The arrows indicate the flow of the fluid.

The microslides used to adjust the distance between the detector fiber and the source fiber had an accuracy of 5 μm. Errors from this adjustment are considered negligeble compared to other potential sources of error.

5.3.4 Reproducibility

The measurements with the lasers are considered more reliable than the measurements with the halogen lamp due to the modulation of the signal (i.e. the use of a lock-in amplifier). The high accuracy and stability of the photon multiplier tube compared to the spectrometer also contributes to the better reliability in the measurements with the lasers. The distances used in the linear fit was determined by the person analysing the data. This may introduce an error which worsens the reproducibility. Calculations with variations in the distances included in the linear fit for the measurement on salmon for needle insertion across several layers with the He-Ne laser was carried out, see table 15. This showed a small error, but the error in the measurements with the halogen lamp will probably be larger.

Measurements with the lasers
Measurements on the fluids yielded standard deviations of less than 3 %. Measurements on salmon yielded standard deviations of less than 20 %. Considering only the measurements with needle insertion, the standard deviation is of less than 10 %. There are less potential sources of error when measuring on fluids compared to measurements on the salmon, and the reproducibility in the measurements on the fluids are very good (except the one performed on the mixture of mashed salmon and intralipid with the YAG laser). The reproducibility in the measurement on salmon is adequate.

Measurements with the halogen lamp
Measurements on the fluids yielded standard deviations up to 10 % for most wavelengths. Compared with the measurements performed with the lasers, there appears to be a systematic error. This will not worsen the reproducibility, but it will worsen the quality in the measurements. The reproducibility in the measurements on the fluids with the halogen lamp is adequate. Measurements on salmon with needle insertion yielded standard deviations up to 60 %, whilst needle extraction yielded standard deviations up to 90 %. The variation in the results for the salmon are large, and the reproducibilities are poor.

5.4 Expenditure of time in the laboratory

Besides the measurements, all the preparations done beforehand were time-consuming. This includes for instance fixing the connectors to the setup for the halogen lamp.

Measurements on intralipid with the lasers
The measurements on solution 1-3 in table 7 with one laser were done in 5-6 hours. Measurement on solution 4 in table 7 was done separately, and took about 2 hours (only YAG laser).

Measurements on salmon with the lasers
In the first measurements on salmon (not included in this report) the measuring values fluctuated significantly, and had a tendency to decrease with time. It was decided to read the value from the lock-in amplifier 1 minute after adjusting the distance between the detector and the source fiber to get consistent results. The measurements across several layers and along one layer in the salmon were done separately, each taking 6-7 hours for each laser. The pre-amplifier was changed twice, and other adjustments were made before starting on the measurements included in this report. After these adjustments the measuring values were much more stable, and did not decrease with time. The procedure of waiting 1 minute after adjusting the distance might have been unnecessary, but it was done as a precaution.

Measurements with the halogen lamp
The integration time in Spectrasuite was set to 5 seconds, and measuring values were averaged over 3 measurements giving a scanning time of 15 seconds. These measurements did not fluctuate as the ones with the lasers, and no waiting time was implemented in the experiments with the salmon. The measurements on solution 1-3 in table 7 were done in 3-4 hours. Measurements on solution 4 in table 7 was done separately, and took about 2 hours. The measurements across several layers and along one layer in the salmon were done separately, each taking 3-4 hours.

5.5 Further work

Measurements on fluids are reproducible, and the variations are within satisfactory limits. However, in the measurements on salmon there are room for improvements. Measurements should be performed while inserting the needle to avoid the effect of the canal made by the detector needle. It is important to be consequent regarding how the needle is inserted into the salmon. This is due to the difference in the penetration depths found from measurements across several layers compared to measurements along one layer. The fat and astaxanthin may be distributed unevenly in the salmon. The measurements should be made on locations in the salmon which is close to each other, but not too close to the canals made by former measurements. The matlab code developed in this thesis requires a person to decide which distances to include in the linear fit. The reproducibility in the results can be improved by making the matlab code choose which distances to include in the linear fit (i.e create a set of rules to select the range for the linear fit).

6 Conclusion

The setup with the lasers yielded results with small variations in measurements on fluids and salmon, and the results are considered to be reproducible. Measurements with the halogen lamp yielded results with larger variations than the setup with the lasers. Measurements on fluids with the halogen lamp showed less variations than measurements on salmon, and are considered to be reproducible. There are more potential sources of error when measuring on the salmon and the setup with the halogen lamp gives less accurate measurements than the setup with the lasers. The results obtained from measurements on salmon with the halogen lamp have a poor reproducibility.

Significant differences were found in the comparison in the results from needle insertion and needle extraction. Measuring on needle extraction yielded larger penetration depths, and larger variations in the results. This is due to the canal made by the detector needle. Measuring on needle insertion is considered to give results closer to the actual penetration depth of the salmon, and is recommended in further work.

Differences were found in the comparison in the results from measuring across several layers and measuring along one layer. Measuring along one layer yielded larger penetration depths. The penetration depth were found to be 6.79 ± 0.33 mm from measurements across several layers and 10.76 ± 1.03 mm along one layer with the He-Ne laser. The absorption and the reduced scattering coefficient were calculated from the measurements with the halogen lamp. The absorption coefficients were approximately equal for all wavelengths included in the result. The reduced scattering coefficient were significantly smaller when measuring along one layer. A hypothesis to explain this is presented in this thesis.

In the calculations of the absorption and the reduced scattering coefficients, the diffusion approximation in radiative transfer theory was used. The validity of the diffusion approximation is dependent on a reduced scattering coefficient much larger than the absorption coefficient. The measurement on salmon with the halogen lamp were highly uncertain, but using these results the diffusion approximation was found to be a good approximation for wavelengths from 600 nm to 700 nm. The diffusion approximation may be a good approximation outside these wavelengths, but due to the large uncertainty in the measurements performed in this thesis a conservative interpretation was made. With further development, it may be possible to determine the astaxanthin content of salmon with the method used in this thesis.

References

[1] H. J. Swatland, J. C. Brooks, and M. F. Miller. Possibilities for predicting taste and tenderness of broiled beef steaks using an optical-electromechanical probe. *Meat science*, 50(1):1–12, 1998.

[2] R. Karoui, A. M. Mouazen, E. Dufour, R. Schoonheydt, and J. De Baerdmaeker. A comparison and joint use of vis-nir and mir spectroscopic methods for the determination of some chemical parameters in soft cheeses at external and central zones: a preliminary study. *European food research and technology*, 223(3):363–371, 2006.

[3] J. F. Frank and G. S. Birth. Application of near infrared reflectance spectroscopy to cheese analysis. *Journal of dairy science*, 65(7):1110–1116, 1982.

[4] Statistical overview of norwegian seafood around the world. Technical report, Norwegian seafood export council, Strandveien 106, PO box 6176, N-9291 Tromsø Norway, 2007.

[5] D. F. Koteng. *Markedsundersøkelse, norsk laks*. Sats & trykk Grafisk Trykk Sotra, 1992.

[6] J. P. Wold and T. Isaksson. Non-destructive determination of fat and moisture in whole atlantic salmon by near-infrared diffuse spectroscopy. *Journal of food science*, 62(4):734–736, 1997.

[7] J. P. Wold, T. Jakobsen, and L. Krane. Atlantic salmon average fat content estimated by near-infrared transmittance spectroscopy. *Journal of food science*, 62(4):734–736, 1997.

[8] Y. Huang, A. G. Cavinato, D. M. Mayes, G. E. Bledsoe, and B. A. Rasco. Nondestructive prediction of moisture and sodium chloride in cold smoked atlantic salmon (salmo salar). *Journal of food science*, 67(7):2543–2547, 2002.

[9] Y. Huang, A. G. Cavinato, D. M. Mayes, L. J. Kangas, G. E. Bledsoe, and B. A. Rasco. Nondestructive determination of moisture and sodium chloride in cured atlantic salmon (salmo salar) (tejin) using short-wavelength near-infrared spectroscopy. *Journal of food science*, 68(2):482–486, 2003.

[10] R. Christiansen, G. Struksnæs, R. Estermann, and O. J. Torrissen. Assessment of flesh colour in atlantic salmon, salmo salar l. *Aquaculture Research*, 26(5):311–321, 1995.

[11] J. P. Wold, B. J. Marquardt, B. K. Dable, D. Robb, and B. Hatlen. Rapid quantification of carotenoids and fat in atlantic salmon (salmo salar l.) by raman spectroscopy and chemometrics. *Applied Spectroscopy*, 58(4):395–403, 2004.

[12] W. F. Cheong, S. A. Prahl, and A. J. Welch. A review of the optical properties of biological tissue. *IEEE Journal of Quantum Electronics*, 26(12):2166–2185, 1990.

[13] J. S. Lilley. *Nuclear Physics: Principles and Applications.* John Wiley & Sons, 2001.

[14] T. Spott. *Characterization of layered tissue structures with diffusely propagating photon-density waves.* PhD thesis, Norwegian University of Science and Technology.

[15] T. Spott and L. O. Svaasand. Collimated light sources in the diffusion approximation. *Applied Optics*, 39(34):6453–6465, 2000.

[16] M. N. Berberan-Santos. Beer's law revisited. *Journal of Chemical Education*, 67(9):757–759, 1990.

[17] C. F. Bohren and D. R. Huffman. *Absorption and Scattering of Light by Small Particles.* John Wiley & Sons, 1983.

[18] V. Tuchin. *Tissue Optics: Light Scattering Methods and Instruments for Medical Diagnosis.* The International Society for Optical Engineering, 2000.

[19] J. R. Lamarsh. *Introduction to Nuclear Reactor Theory.* Addison-Wesley, 1966.

[20] C. Angell and B. E. Lian. *Fysiske størrelser og enheter.* Universitetsforlaget, 2004.

[21] K. M. Case and P. F. Zweifel. *Linear Transport Theory.* Addison-Wesley, 1967.

[22] J. B. Fishkin, S. Fantini, M. J. van de Ven, and E. Gratton. Gigahertz photon density waves in a turbid medium: Theory and experiments. *Physical review E*, 53(3):2307–2319, 1996.

[23] A. Ishimaru. Diffusion of light in turbid media. *Applied Optics*, 28(12):2210–2215, 1989.

[24] R. C. Haskell, L. O. Svaasand, T. T. Tsay, T. C. Feng, M. S. McAdams, and B. J. Tromberg. Boundary conditions for the diffusion equation in radiative transfer. *Journal of the Optical Society of America*, 11(10):2727–2741, 1994.

[25] L. O. Svaasand and R. Ellingsen. Optical properties of human brain. *Photochemistry and Photobiology*, 38(3):293–299, 1983.

[26] A. J. Welch and M. J. C. van Gemert, editors. *Optical-Thermal Response of Laser-Irradiated Tissue.* Plenum Press, 1995.

[27] G. I. Page and S. J. Davies. Hepatic carotenoid uptake in rainbow trout (oncorhynchus mykiss) using an isolatedorgan perfusion model. *Aquaculture*, 225(1-4):405–419, 2003.

[28] G. Britton, R. J. Weesie, D. Askin, J. D. Warburton, L. Gallardo-Guerrero, F. J. Jansen, H. J. M. de Groot, J. Lugtenburg, J. P. Cornard, and J. C. Merlin. Cartenoid blues: Structural studies on cartenoproteins. *Pure and Applied Chemistry*, 69(10):2075–2084, 1997.

[29] L. L. Randeberg, A. J. D. Hagen, and L. O. Svaasand. Optical properties of human blood as a function of temperature. *Proceedings of SPIE - The International Society for Optical Engineering*, 4609:20–28, 2002.

[30] A. J. D. Hagen. Optiske egenskaper i blod og vev. Master's thesis, Norwegian University of Science and Technology, february 2001.

[31] C. J. M. Moes, M. J. C. van Gemert, W. M. Star, J. P. A. Marijnissen, and S. A. Prahl. Measurements and calculations of the energy fluence rate in a scattering and absorbing phantom at 633 nm. *Applied Optics*, 28(12):2292–2296, 1989.

[32] H. J. van Staveren, C. J. M. Moes, J. van Marle, S. A. Prahl, and M. J. C. van Gemert. Light scattering in intralipid-10% in the wavelength range of 400-1100 nm. *Applied Optics*, 30(31):4507–4514, 1991.

[33] R. Michels, F. Foschum, and A. Kienle. Optical properties of fat emulsions. *Optics Express*, 16(8):5907–5925, 2008.

[34] R. M. Pope and E. S. Fry. Absorption spectrum (380-700 nm) of pure water. ii. integrating cavity measurements. *Applied Optics*, 36(33):8710–8723, 1997.

[35] T. Mørkøre, J. L. Vallet, M. Cardinal, M. C. Gomez-Guillen, P. Montero, O. J. Torrissen, R. Nortvedt, S. Sigurgisladottir, and M. S. Thommasen. Fat content and fillet shape of atlantic salmon: Relevance for processing yield and quality of raw and smoked products. *Journal of food science*, 66(9):1348–1354, 2001.

A Appendix

A.1 Measurements on intralipid and ink, solution 3 in table 7

The results from these measurements were not used in the calculations. The natural logarithm to the fluence rate times distance, $\ln(\phi r)$, is plotted as a function of distance, r, in the result for the lasers. The result from the measurements are plotted in figure 38 for the YAG laser and figure 39 for the He-Ne laser. The penetration depth for the YAG laser was 4.26±0.08mm, and 5.00±0.09mm for the He-Ne laser. The distances included in the linear fit are shown in table 17. The penetration depth is plotted as a function of wavelength for the measurement with the halogen lamp in figure 40.

Table 17: Distances used in the linear fit

Light source	Distances used in the linear fit (mm)
YAG laser	6-20
He-Ne laser	6-20
Halogen lamp	9-14

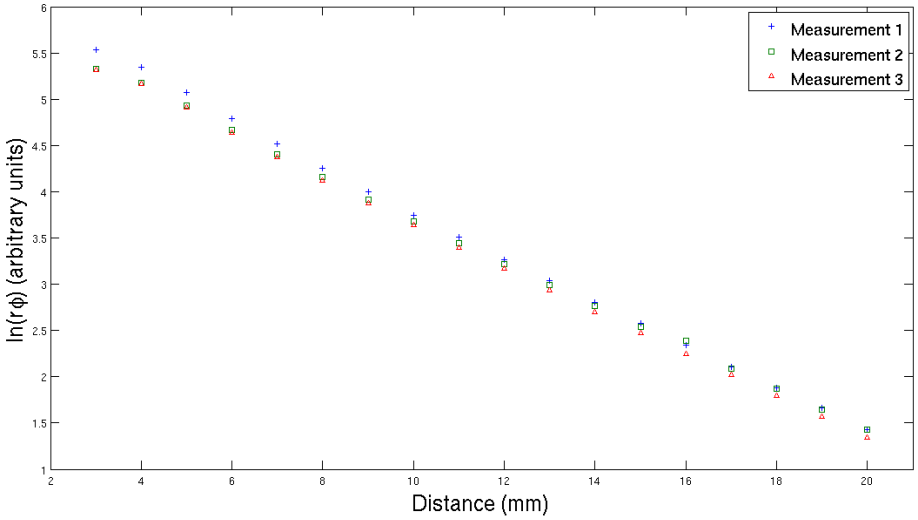

Figure 38: The natural logarithm to the distance times fluence rate, $\ln(r\phi)$, as a function of distance, r, for intralipid. Three measurements were performed. Light source: YAG laser.

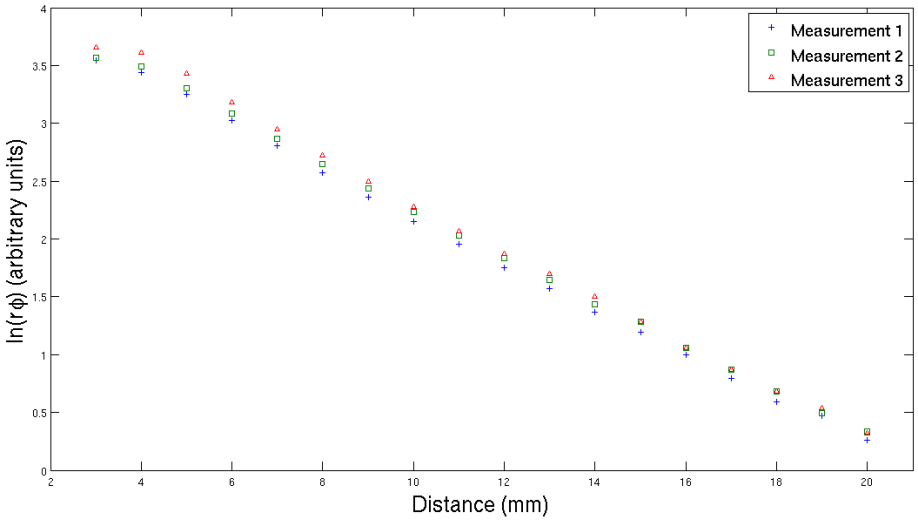

Figure 39: The natural logarithm to the distance times fluence rate, $\ln(r\phi)$, as a function of distance, r, for intralipid. Three measurements were performed. Light source: He-Ne laser.

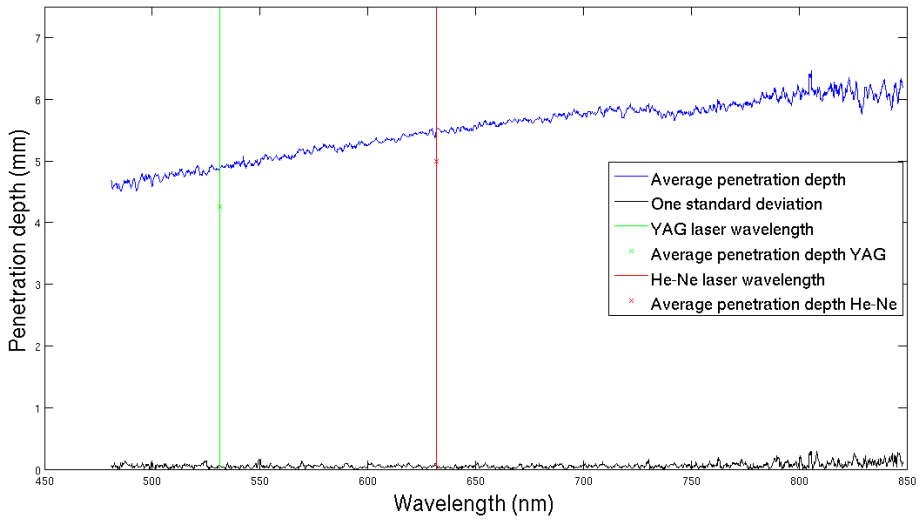

Figure 40: The penetration depth, δ, as a function of wavelength, λ, for the mixture of ink and intralipid (solution 2 in table 7). The blue upper curve is the average of the meaurements, while the lower black curve is the standard deviation of the measurements. The vertical lines and the "x" represent the wavelength and the result from the He-Ne laser and the Yag laser. Three measurements were performed. Light source: Halogen lamp.

A.2 Reflection spectrum and fluorescence spectrum of the salmon

The reflection spectrum was measured with a similar setup to the one described in section 3.2. The detector fiber and the source fiber was held by hand close to the surface of the salmon. The angle between the detector fiber and the source fiber was about 90 degrees. The same halogen lamp was used, but another spectrometer was used. An Ocean optics SD2000 fiber optic spectrometer was used. In the measurement of the fluorescence spectrum, the halogen lamp was replaced by a UV laser from Laser Science, model VSL-337ND. The reflection spectrum of the salmon is plotted in figure 41. The vertical lines represents the wavelength to the laser used in the experiments. The fluorescence spectrum of the salmon is plotted in figure 42. The vertical line to the left represents the wavelength to the UV-laser used. The other two vertical lines represents the wavelengths to the lasers used in the experiments.

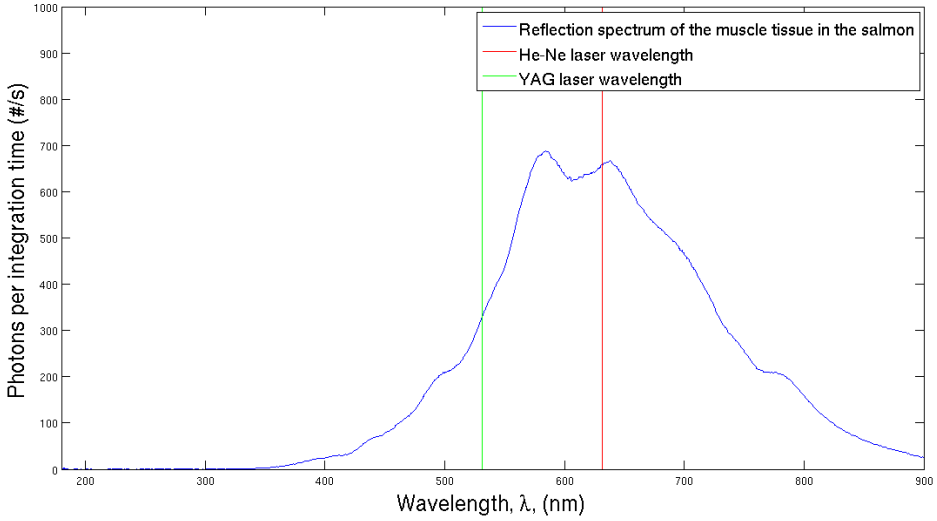

Figure 41: The reflection spectrum to the muscle tissue in the salmon. The vertical lines represents the wavelength of the He-Ne laser and the YAG laser.

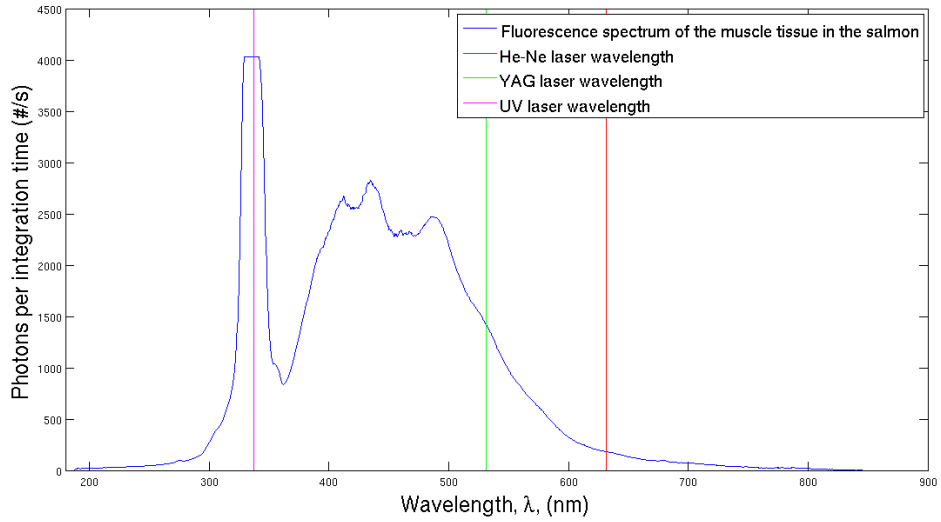

Figure 42: The fluorescence spectrum to the muscle tissue in the salmon. The vertical lines represents the wavelength of the He-Ne laser, the YAG laser and the UV laser.

A.3 Matlab functions

Several matlab functions has been made when analysing the data obtained from the measurements. Most of the functions are described in this section. All matlab files used, and data obtained from the measurements are attached electronically. In the measurements with the halogen lamp, huge amounts of data were produced. To plot the penetration depths, the absorption coefficient or the reduced scattering coefficient, it is necessary to load the data into 3d-matrices first. The loading files returns a string with the names of the matrices which the data has been stored in. Theses matrices are used as input in the functions made in this thesis. Small modifications in these functions were made to write the calculated data to ASCII-files. The code is tested in Ubuntu, and works with Matlab version 7.5.0 (R2007b).

A.3.1 Halogen lamp

Matlab file penetrationDepth.m

- Inputs; three 3-dimensional matrices, two integers
- Outputs; none

The matrices corresponding to the measurements which is going to be analysed are entered. The first integer entered, is the number of points to include in the linear fit, and the second integer is the minimum distance to start the linear fit from. Assuming the function returnlimits.m does not change the minimum distance, the integers 6,8 gives a linear fit from 8 mm to 13 mm. This function plots the average penetration depth and the standard deviation as a function of wavelength.

Matlab file penetrationDepth2.m

- Inputs; six 3-dimensional matrices, two integers
- Outputs; none

Same as penetrationDepth.m, except six matrices are entered. This is due to the six measurements performed on the mixture of mashed salmon and intralipid.

Matlab file finnIndeksBolge.m

- Inputs; a double value
- Outputs; a 2-dimensional matrix

This function returns the index for the wavelengths close to the wavelength entered in the function. The value entered is the wavelength in nm, and has to be in the interval 179.14 nm to 885.68 nm.

Matlab file plotForEnBolge.m

- Inputs; three 3-dimensional matrices, integer
- Outputs; none

This function plots the natural logarithm to the distance times fluence rate as a function of distance for one wavelength. The integer entered is the index to the wavelength which is desirable to investigate.

Matlab file muAOgmuSLaks.m

- Inputs; six 3-dimensional matrices, two integers, three 3-dimensional matrics, two integers
- Outputs; none

The six first matrices entered has to be the measurements from the mashed salmon and intralipid. The next two integers are the number of points to include in the linear fit and the minimum distance included in the fit for the measurements on mashed salmon and intralipid. The next three matrices has to be measurements on salmon. And the next two integers are the number of points to include in the linear fit and the minimum distance included in the fit for the measurements on salmon. The function is dependent on data stored in a ASCII-file called "muSIntralipid.txt" This file has to be updated if other reduced scattering coefficients for intralipid are to be used in the calculations.

Matlab file muAOgmuSIntralipid.m

- Inputs; three 3-dimensional matrices, two integers
- Outputs; none

The three matrices entered has to be measurements on solution 3 in table 7. This function is dependent on data from the absorbance of ink stored in ASCII-files. If the function is to calculate the coefficients for intralipid based on results from solution 2 in table 7, small modifications has to be made. The function plots the coefficients for intralipid as a function of wavelength.

A.3.2 Miscellaneous

Matlab file average.m

- Inputs; a 2-dimensional matrix
- Outputs; a vector

The average of each row in the entered 2-dimensional matrix is found. The function returns a vector with the average values.

Matlab file fwhm.m

- Inputs; a matrix with two columns
- Outputs; a vector

The function is designed to find the FWHM of the laser spectrum measured with the spectrometer used in the experiments. It returns relevant values in further calculations.

Matlab file maxKolonne.m

- Inputs; a matrix with two columns
- Outputs; a vector

The function is designed to find the peak wavelength of a laser. Reads in the data obtained from measurements with the spectrometer.

A.4 The spectrum and the stability of the Lasers

The stability was measured using a PIN-detector. The PIN-detector was connected to the lock-in amplifier and the same chopper as in the measurements with the lasers was used. The lock-in amplifier was connected to a computer, and a Labview program recorded the measuring value every 20 seconds. The stability was measured over a periode of 25 hours for the He-Ne laser and 30 hours for the YAG laser. The stabilities are shown in figure 43 and 44. The vertical line to the left in the plots is the minimum warm up time used in the experiments.

The spectrum of the lasers was measured using a fiber optic spectrometer (Ocean optics, USB4000) with pertaining software. The spectrum of the lasers are shown in figure 45. The He-Ne laser has a peak at 631.79 nm and a FWHM of 5.68 nm. The Yag laser has a peak at 531.24 nm and a FWHM of 7.46 nm. The characteristics of the lases are summarized in table 1.

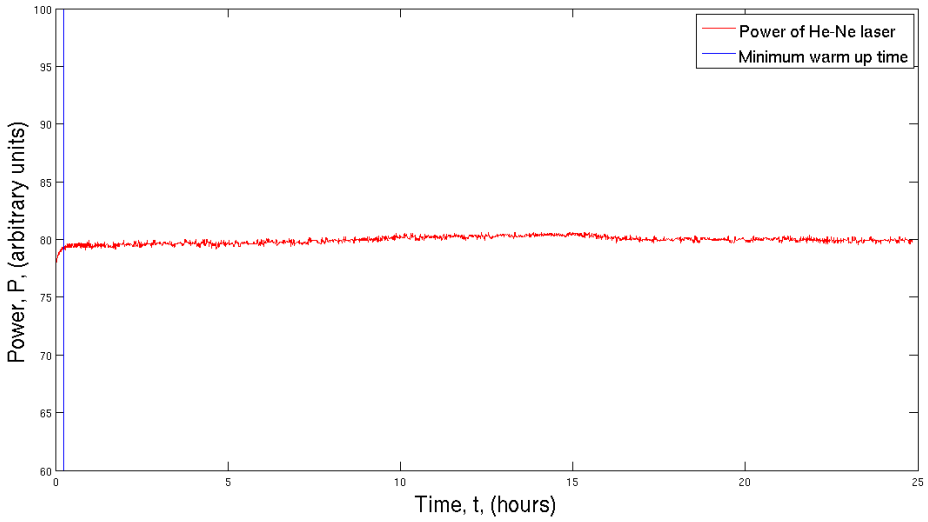

Figure 43: Stability of the He-Ne laser

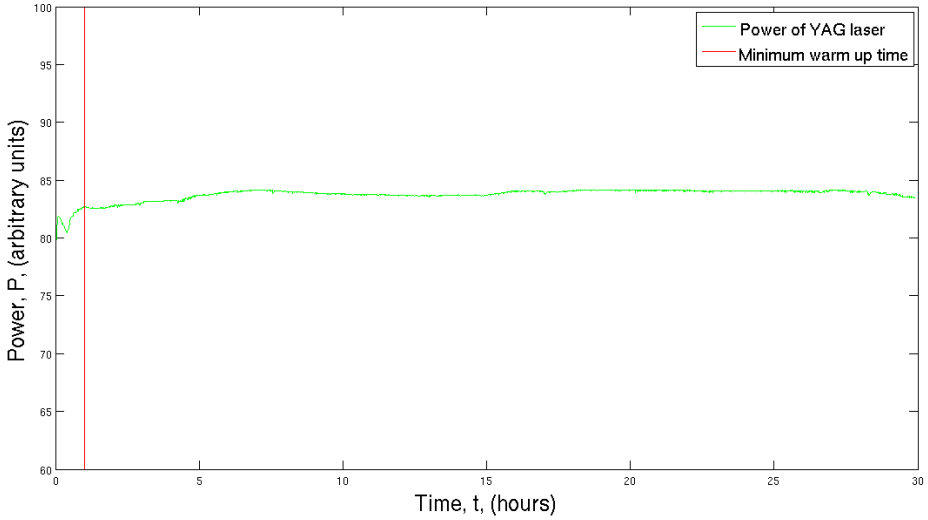

Figure 44: Stability of the Yag laser

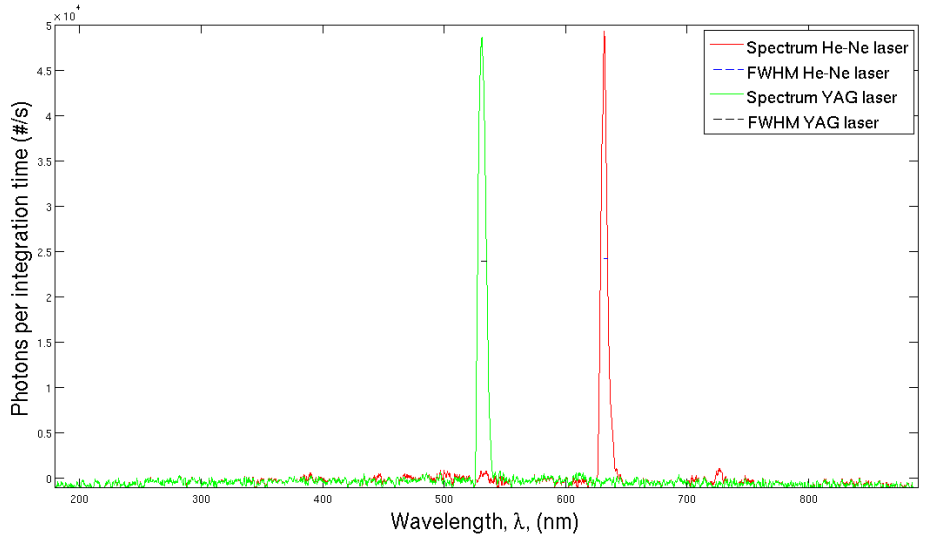

Figure 45: The spectrum and FWHM for the He-Ne laser and the YAG laser

A.5 Technical specifications

II - 1

SECTION II - SPECIFICATIONS

NOTE: Allow a 15 minute warm-up period when first applying power to the unit.

Sensor Readout *

Operating Temperature Range	:	14 degrees C to 40 degrees C
Overall accuracy at 27 degrees C Ambient	:	+/- .1% (+/- .001 digital)
Linearity	:	.05%
Gain Drift vs Temperature	:	0.07%/degrees C
Zero Drift	:	+/- .001 digital

BCD Output Description

The parallel BCD output lines are at +5V logic level (positive logic), capable of driving 2 LPTTL loads.

The multiplexed BCD output lines are at +5V logic level (negative logic), capable of driving 4 CMOS loads. The load pulses are at +5V logic level (positive logic), capable of driving 2 CMOS loads.

* NOTE: These specifications pertain to the readout circuit only. The performance of the entire system is limited by that of the photosensors.

Figure 46: Technical specifications, photon multiplier tube, page 1 of 2

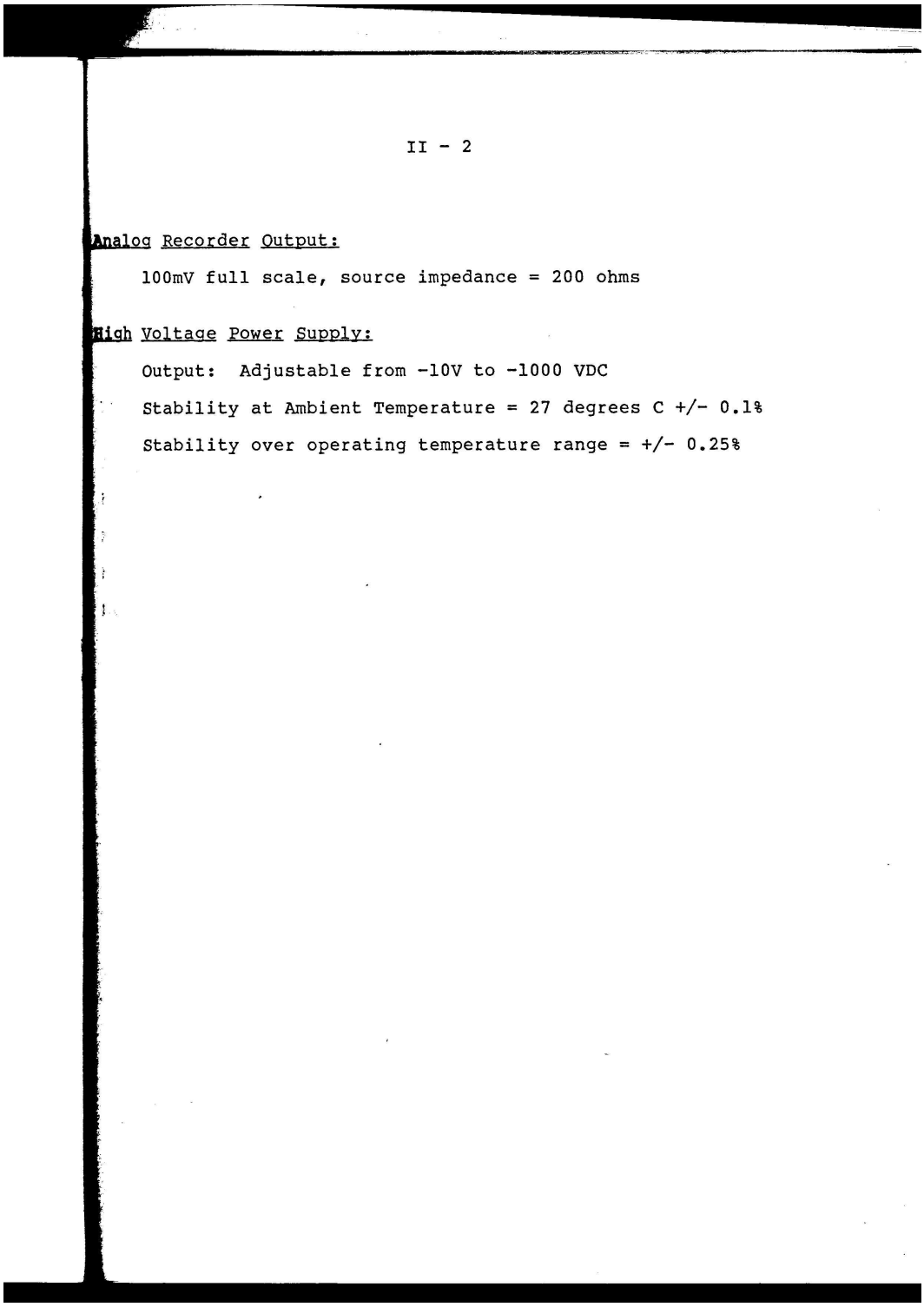

II - 2

Analog Recorder Output:

100mV full scale, source impedance = 200 ohms

High Voltage Power Supply:

Output: Adjustable from -10V to -1000 VDC

Stability at Ambient Temperature = 27 degrees C +/- 0.1%

Stability over operating temperature range = +/- 0.25%

Figure 47: Technical specifications, photon multiplier tube, page 2 of 2

SR830 DSP LOCK-IN AMPLIFIER

SPECIFICATIONS

SIGNAL CHANNEL

Voltage Inputs	Single-ended (A) or differential (A-B).
Current Input	10^6 or 10^8 Volts/Amp.
Full Scale Sensitivity	2 nV to 1 V in a 1-2-5-10 sequence (expand off).
Input Impedance	Voltage: 10 MΩ+25 pF, AC or DC coupled. Current: 1 kΩ to virtual ground.
Gain Accuracy	±1% from 20°C to 30°C (notch filters off), ±0.2 % Typical.
Input Noise	6 nV/√Hz at 1 kHz (typical).
Signal Filters	60 (50) Hz and 120(100) Hz notch filters (Q=4).
CMRR	100 dB to10 kHz (DC Coupled), decreasing by 6db/octave above 10 kHz
Dynamic Reserve	Greater than 100 dB (with no signal filters).
Harmonic Distortion	-80 dB.

REFERENCE CHANNEL

Frequency Range	1 mHz to 102 kHz
Reference Input	TTL (rising or falling edge) or Sine. Sine input is1 MΩ, AC coupled (>1 Hz). 400 mV pk-pk minimum signal.
Phase Resolution	0.01°
Absolute Phase Error	<1°
Relative Phase Error	<0.01°
Orthogonality	90° ± 0.001°
Phase Noise	External synthesized reference: 0.005° rms at 1 kHz, 100 ms, 12 dB/oct. Internal reference: crystal synthesized, <0.0001° rms at 1 kHz.
Phase Drift	<0.01°/°C below 10 kHz <0.1°/°C to 100 kHz
Harmonic Detect	Detect at Nxf where N<19999 and Nxf<102 kHz.
Acquisition Time	(2 cycles + 5 ms) or 40 ms, whichever is greater.

DEMODULATOR

Zero Stability	Digital displays have no zero drift on all dynamic reserves. Analog outputs: <5 ppm/°C for all dynamic reserves.
Time Constants	10 µs to 30 s (reference > 200 Hz). 6, 12, 18, 24 dB/oct rolloff. up to 30000 s (reference < 200 Hz). 6, 12, 18, 24 dB/oct rolloff. Synchronous filtering available below 200 Hz.
Harmonic Rejection	-80 dB

INTERNAL OSCILLATOR

Frequency	1 mHz to 102 kHz.
Frequency Accuracy	25 ppm + 30 µHz
Frequency Resolution	4 1/2 digits or 0.1 mHz, whichever is greater.
Distortion	f<10 kHz, below -80 dBc. f>10 kHz, below -70 dBc.1 Vrms amplitude.
Output Impedance	50 Ω
Amplitude	4 mVrms to 5 Vrms (into a high impedance load) with 2 mV resolution. (2 mVrms to 2.5 Vrms into 50Ω load).
Amplitude Accuracy	1%
Amplitude Stability	50 ppm/°C
Outputs	Sine output on front panel. TTL sync output on rear panel. When using an external reference, both outputs are phase locked to the external reference.

Figure 48: Technical specifications, lock-in amplifier, page 1 of 2

SR830 DSP Lock-In Amplifier

DISPLAYS

Channel 1	4 1/2 digit LED display with 40 segment LED bar graph. X, R, X Noise, Aux Input 1 or 2. The display can also be any of these quantities divided by Aux Input 1 or 2.
Channel 2	4 1/2 digit LED display with 40 segment LED bar graph. Y, θ, Y Noise, Aux Input 3 or 4. The display can also be any of these quantities divided by Aux Input 3 or 4.
Offset	X, Y and R may be offset up to ±105% of full scale.
Expand	X, Y and R may be expanded by 10 or 100.
Reference	4 1/2 digit LED display. Display and modify reference frequency or phase, sine output amplitude, harmonic detect, offset percentage (X, Y or R), or Aux Outputs 1-4.
Data Buffer	16k points from both Channel 1 and Channel 2 display may be stored internally. The internal data sample rate ranges from 512 Hz down to 1 point every 16 seconds. Samples can also be externally triggered. The data buffer is accessible only over the computer interface.

INPUTS AND OUTPUTS

Channel 1 Output	Output proportional to Channel 1 display, or X. Output Voltage: ±10 V full scale. 10 mA max output current.
Channel 2 Output	Output proportional to Channel 2 display, or Y. Output Voltage: ±10 V full scale. 10 mA max output current.
X and Y Outputs	Rear panel outputs of cosine (X) and sine (Y) components. Output Voltage: ±10 V full scale. 10 mA max output current.
Aux. Outputs	4 BNC Digital to Analog outputs. ±10.5 V full scale, 1 mV resolution. 10 mA max output current.
Aux. Inputs	4 BNC Analog to Digital inputs. Differential inputs with1 MΩ input impedance on both shield and center conductor. ±10.5 V full scale, 1 mV resolution.
Trigger Input	TTL trigger input triggers stored data samples.
Monitor Output	Analog output of signal amplifiers (before the demodulator).

GENERAL

Interfaces	IEEE-488 and RS232 interfaces standard. All instrument functions can be controlled through the IEEE-488 and RS232 interfaces.
Preamp Power	Power connector for SR550 and SR552 preamplifiers.
Power	40 Watts, 100/120/220/240 VAC, 50/60 Hz.
Dimensions	17"W x 5.25"H x 19.5"D
Weight	30 lbs.
Warranty	One year parts and labor on materials and workmanship.

Figure 49: Technical specifications, lock-in amplifier, page 2 of 2

Shanghai Dream Lasers Technology Co., Ltd.

10mW SLM Green Laser Modules

Specifications

Model Number	SLM-532-SLM-010
Series Number	74525
Output Power	16mW
Output Wavelength	532nm
Beam Mode	TEM00, CW
Longitude Mode	Single
Power Stability	<±5% (r.m.s. over 8 hours)
Output Noise (r.m.s, 10Hz - 20MHz)	0.2%
LD Drive Current	550mA
LD Drive Current Limit	750mA
Beam Divergence	<1.0mrad
Beam Diameter	<1.0mm
Coherent Length (m)	>50m
Spectra Linewidth	<0.00001nm
Point Stability	0.05mrad
Expected Lifetime (hours)	10,000 hours
Warm Up time	<15 minutes
Operating Temperature	15℃~35℃
Dimension of laser head	156 (L) x 73 (W) x 46.2 (H)

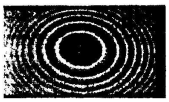

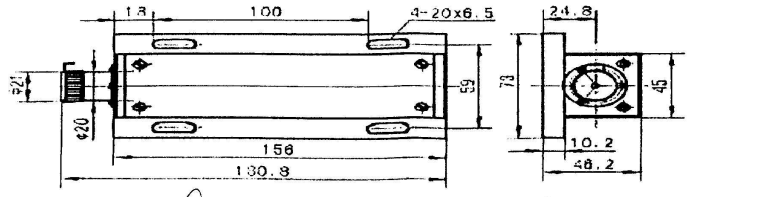

Tested by Serena Date Aug 09, 2005

Checked by Date

Tel: +86-21-66403972 Fax: +86-21-66342597 www.dreamlasers.com sales@dreamlasers.com

Figure 50: Technical specifications, YAG laser, page 1 of 1

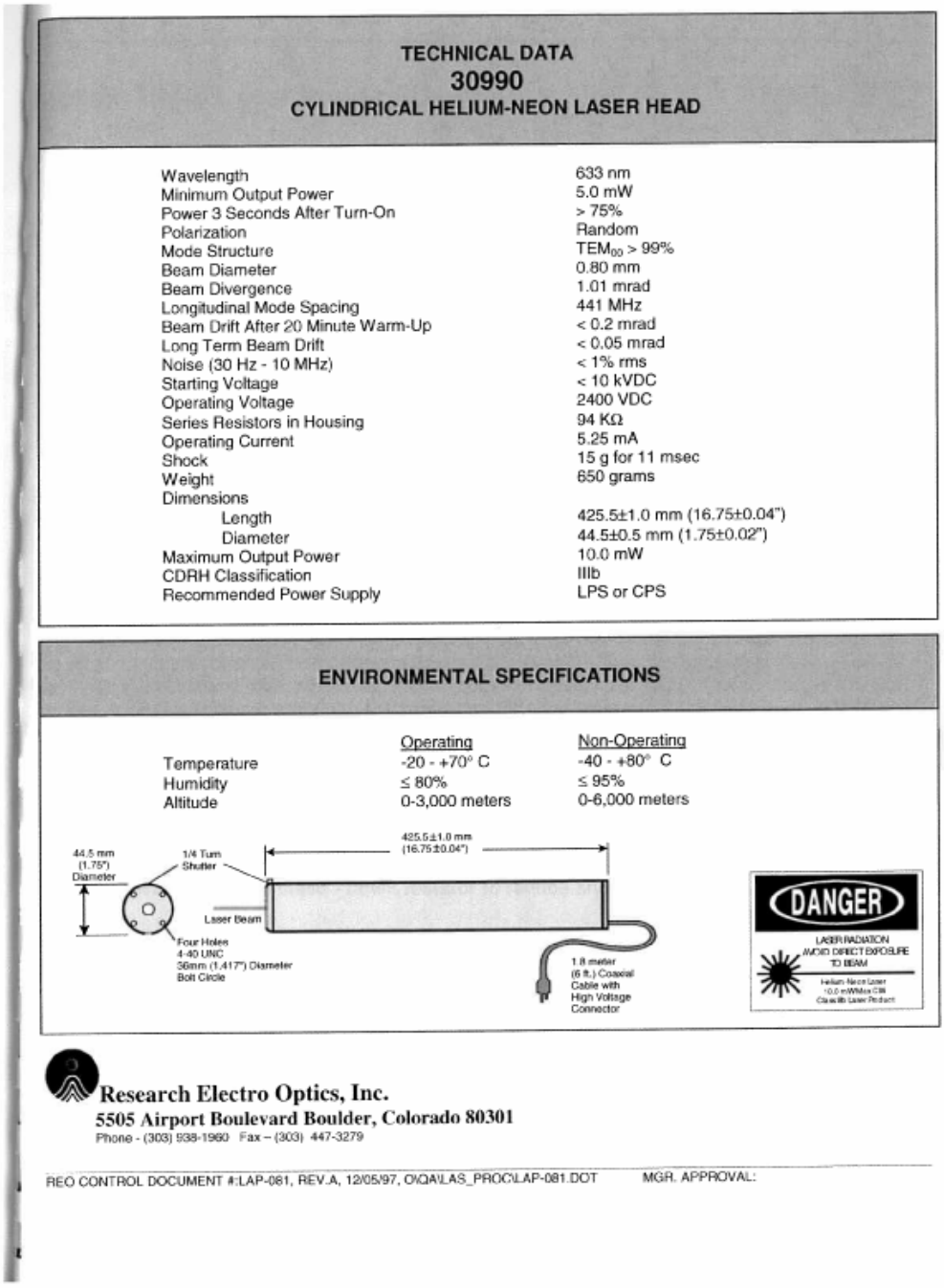

TECHNICAL DATA
30990
CYLINDRICAL HELIUM-NEON LASER HEAD

Wavelength	633 nm
Minimum Output Power	5.0 mW
Power 3 Seconds After Turn-On	> 75%
Polarization	Random
Mode Structure	TEM_{00} > 99%
Beam Diameter	0.80 mm
Beam Divergence	1.01 mrad
Longitudinal Mode Spacing	441 MHz
Beam Drift After 20 Minute Warm-Up	< 0.2 mrad
Long Term Beam Drift	< 0.05 mrad
Noise (30 Hz - 10 MHz)	< 1% rms
Starting Voltage	< 10 kVDC
Operating Voltage	2400 VDC
Series Resistors in Housing	94 KΩ
Operating Current	5.25 mA
Shock	15 g for 11 msec
Weight	650 grams
Dimensions	
Length	425.5±1.0 mm (16.75±0.04")
Diameter	44.5±0.5 mm (1.75±0.02")
Maximum Output Power	10.0 mW
CDRH Classification	IIIb
Recommended Power Supply	LPS or CPS

ENVIRONMENTAL SPECIFICATIONS

	Operating	Non-Operating
Temperature	-20 - +70° C	-40 - +80° C
Humidity	≤ 80%	≤ 95%
Altitude	0-3,000 meters	0-6,000 meters

Research Electro Optics, Inc.
5505 Airport Boulevard Boulder, Colorado 80301
Phone - (303) 938-1960 Fax – (303) 447-3279

REO CONTROL DOCUMENT #:LAP-081, REV.A, 12/05/97, O:\QA\LAS_PROC\LAP-081.DOT MGR. APPROVAL:

Figure 51: Technical specifications, HeNe laser, page 1 of 1

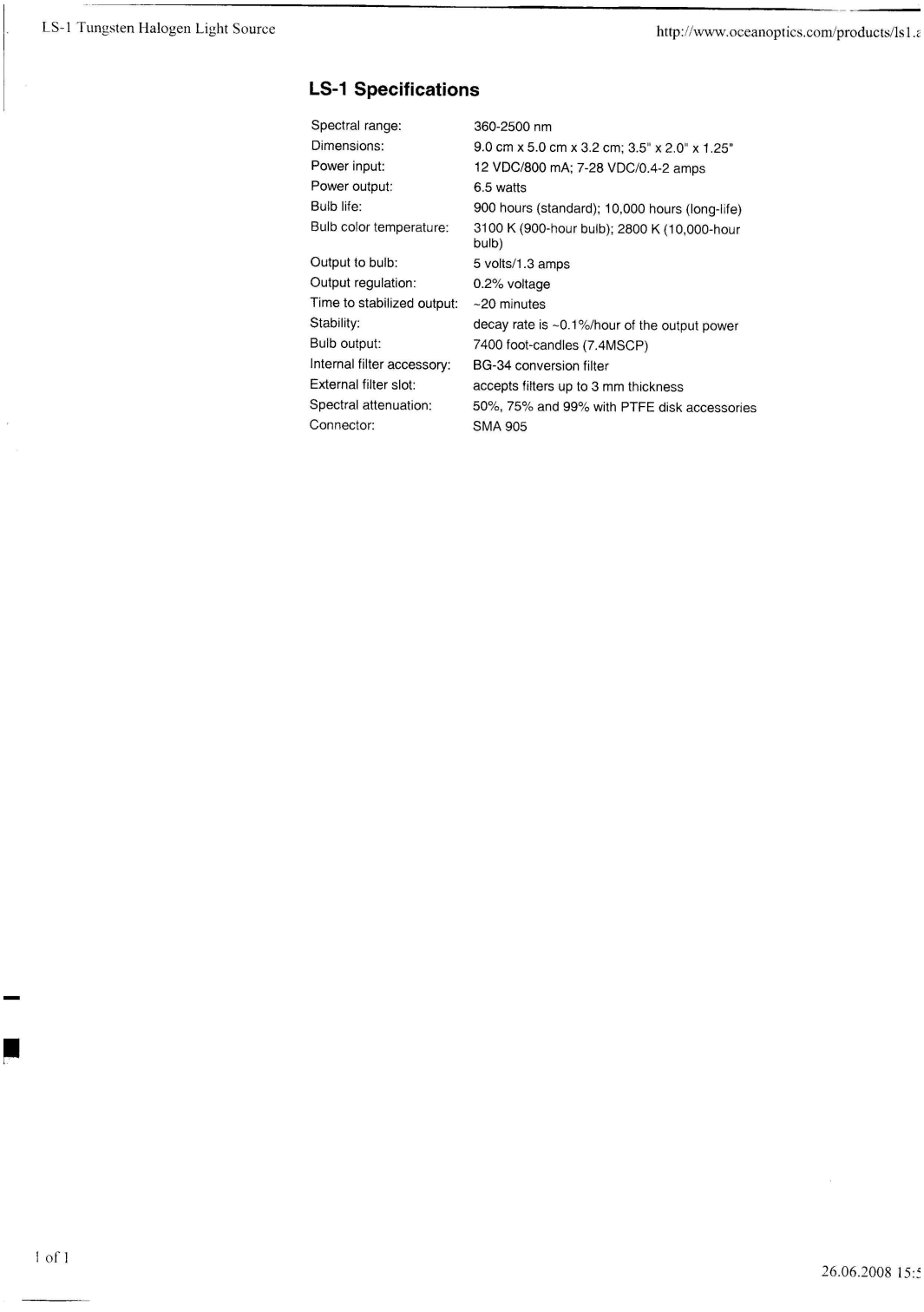

LS-1 Tungsten Halogen Light Source http://www.oceanoptics.com/products/ls1.a

LS-1 Specifications

Spectral range:	360-2500 nm
Dimensions:	9.0 cm x 5.0 cm x 3.2 cm; 3.5" x 2.0" x 1.25"
Power input:	12 VDC/800 mA; 7-28 VDC/0.4-2 amps
Power output:	6.5 watts
Bulb life:	900 hours (standard); 10,000 hours (long-life)
Bulb color temperature:	3100 K (900-hour bulb); 2800 K (10,000-hour bulb)
Output to bulb:	5 volts/1.3 amps
Output regulation:	0.2% voltage
Time to stabilized output:	~20 minutes
Stability:	decay rate is ~0.1%/hour of the output power
Bulb output:	7400 foot-candles (7.4MSCP)
Internal filter accessory:	BG-34 conversion filter
External filter slot:	accepts filters up to 3 mm thickness
Spectral attenuation:	50%, 75% and 99% with PTFE disk accessories
Connector:	SMA 905

1 of 1 26.06.2008 15:5

Figure 52: Technical specifications, tungsten halogen lamp, page 1 of 1

Specifications

Physical	
Dimensions:	89.1 mm x 63.3 mm x 34.4 mm
Weight:	190 grams
Detector Specifications	
Detector:	Toshiba TCD1304AP Linear CCD array
Detector range:	200-1100 nm
Pixels:	3648 pixels
Pixel size:	8 µm x 200 µm
Pixel well depth:	100,000 electrons
Signal-to-noise ratio:	300:1 (at full signal)
A/D resolution:	16 bit
Dark noise:	50 RMS counts
Corrected linearity:	< 0.2%
Sensitivity:	130 photons/count at 400 nm; 60 photons/count at 600 nm
Optical Bench	
Design:	f/4, Asymmetrical crossed Czerny-Turner
Focal length:	42 mm input; 68 mm output
Entrance aperture:	5, 10, 25, 50, 100 or 200 µm wide slits or fiber (no slit)
Grating options:	14 different grating options, UV through Shortwave NIR
HC-1 grating option:	No
Detector collection lens option:	Yes, L4
DET4 filter options:	DET4-200-850; DET4-350-1000
Other bench filter options:	Longpass OF-1 filters
Collimating and focusing mirrors:	Standard or SAG+UPG
UV enhanced window:	Yes, UV4
Fiber optic connector:	SMA 905 to 0.22 numerical aperture single-strand optical fiber
Spectroscopic	
Wavelength range:	Grating dependent
Optical resolution:	~0.3-10.0 nm FWHM (grating dependent)
Signal-to-noise ratio:	300:1 (at full signal)
A/D resolution:	16 bit
Dark noise:	50 RMS counts
Integration time:	3.8 milliseconds to 10 seconds
Dynamic range:	2 x 10^8 (system), 1300:1 for a single acquisition
Stray light:	<0.05% at 600 nm; 0.10% at 435 nm
Electronics	
Power consumption:	250 mA @ 5 VDC
Data transfer speed:	Full spectrum to memory every 5 ms with USB 2.0 port
Inputs/Outputs:	Yes, 8 onboard digital user-programmable GPIOs
Analog channels:	No
Auto nulling:	Yes
Breakout box compatible:	Yes, HR4-BREAKOUT
Trigger modes:	4 modes
Strobe functions:	Yes
Connector:	22-pin connector
Computer	
Operating systems:	Windows 98/Me/2000/XP, Mac OS X and Linux with USB port; Any 32-bit Windows OS with serial port
Computer interfaces:	USB 2.0 @ 480 Mbps (USB1.1 compatible); RS-232

Figure 53: Technical specifications, fiber optic spectrometer (USB4000), page 1 of 2

	(2-wire) @ 115.2 K baud
Peripheral interfaces:	SPI (3-wire); I2C inter-integrated circuit

Serial port operation tips: When using the serial port, the USB4000 requires a single 5-volt power supply (not included). Also, SpectraSuite Spectroscopy Software does not support spectrometer operation via the serial port. However, using the included Serial Port Command Set, you can write your own software that makes serial port operation possible.

Figure 54: Technical specifications, fiber optic spectrometer (USB4000), page 2 of 2